



Effects of CO₂ flushing on crystal textures and compositions: experimental evidence from recent K-trachybasalts erupted at Mt. Etna

This is a pre print version of the following article:

Original:

Giuffrida, M., Holtz, F., Vetere, F., Viccaro, M. (2017). Effects of CO₂ flushing on crystal textures and compositions: experimental evidence from recent K-trachybasalts erupted at Mt. Etna. CONTRIBUTIONS TO MINERALOGY AND PETROLOGY, 172(11-12) [10.1007/s00410-017-1408-3].

Availability:

This version is available <http://hdl.handle.net/11365/1251059> since 2023-12-12T10:00:05Z

Published:

DOI:10.1007/s00410-017-1408-3

Terms of use:

Open Access

The terms and conditions for the reuse of this version of the manuscript are specified in the publishing policy. Works made available under a Creative Commons license can be used according to the terms and conditions of said license.

For all terms of use and more information see the publisher's website.

(Article begins on next page)

Effects of CO₂ flushing on crystal textures and compositions: experimental evidence from recent K-trachybasalts erupted at Mt. Etna

Marisa Giuffrida¹, Francois Holtz², Francesco Vetere³, Marco Viccaro^{1,4}

¹ *Università di Catania, Dipartimento di Scienze Biologiche, Geologiche e Ambientali – Sezione di Scienze della Terra, Corso Italia 57, I-95129, Catania, Italy*

² *Leibniz Universität Hannover, Institut of Mineralogy, Callinstr. 3, D-30167 Hannover*

³ *Università di Perugia, Dipartimento di Fisica e Geologia, Piazza Università 1, Perugia, Italy*

⁴ *Istituto Nazionale di Geofisica e Vulcanologia, Osservatorio Etneo, Piazza Roma 2, I-95125, Catania Italy*

Abstract

Changes in magmatic assemblages and crystal stability as a response of CO₂-flushing in basaltic systems have been never directly addressed experimentally, making the role of CO₂ in magma dynamics still controversial and object of scientific debate. We conducted a series of experiments to understand the response of magmas from Etna volcano to CO₂ flushing. We performed a first experiment at 300 MPa to synthesize a starting material composed of crystals of some hundreds of μm and melt pools. This material is representative of an initial magmatic assemblage composed of plagioclase, clinopyroxene and a water-undersaturated melt with 1.6 wt.% H₂O. In a second step, the initial assemblage was equilibrated at 300 and 100 MPa with fluids having different XCO₂^{fl} (CO₂/(H₂O + CO₂)). At low XCO₂^{fl} (< 0.2 to 0.4), plagioclase is completely dissolved and clinopyroxene show dissolution textures. For relatively high XCO₂^{fl} (0.9 at 300 MPa), the flushing of a CO₂-rich fluid phase leads to an increase of the amount of clinopyroxene and a decrease of the abundance of plagioclase at 300 MPa. This decrease of plagioclase proportion is associated with a change in An content.

Our experiments demonstrate that flushing basaltic systems with fluids may drastically affect crystal textures and phase equilibria depending on the amount of H₂O-CO₂ in the fluid phase. Since

texture and crystal proportions are among the most important parameters governing the rheology of magmas, fluid flushing will also influence magma ascent to the Earth's surface. The experimental results open new perspectives to decipher the textural and compositional record of minerals observed in volcanic rocks from Mt. Etna, and at the same time offer the basis for interpreting the information preserved in minerals from other basaltic volcanoes erupting magmas enriched in CO₂

Keywords: Mt. Etna, crystallization experiments, CO₂ flushing, crystal textures.

1. Introduction

Processes of gas escape and changing concentration of volatiles in natural magmas provide the driving force for volcanic eruptions, as volatiles control the physical melt properties and phase equilibria, with far-reaching implications for magma ascent dynamics and eruptive styles (e.g., Sparks and Pinkerton 1978; Papale and Dobran 1994; Dingwell 1998; Papale 1998; Blundy and Cashman 2001; Sparks et al. 2003; Cashman 2004; Webster et al. 2015). Magmatic volatile composition is typically dominated by H₂O and CO₂. These two components behave quite differently in the melt phase during ascent, due to their strong pressure-dependent and contrasting solubilities (e.g., Brey 1976; Papale 1997; Webster et al. 1999; Newman and Lowenstern 2002; Vetere et al. 2011; Iacono-Marziano et al. 2012; Witham et al. 2012; Vetere et al. 2014; Shishkina et al. 2014a; 2014b). While the central influence of water on volcanic processes has been recognized since decades (e.g., Tuttle and Bowen 1958), the role of CO₂ has only recently been considered to play a central role in magmatic and volcanic dynamics (e.g., Wilson et al. 1980; Spera 1981; 1984; Papale and Polacci 1999; Aiuppa et al. 2007; Blundy et al. 2010; Nicotra and Viccaro 2012). In particular, understanding the behavior of mixed H₂O-CO₂ volatile components in experimental studies has become one of the key to unravel the effects of ascent rates on the kinetics of magma vesiculation and crystallization, along with their implications on eruption mechanisms (e.g., Mourtada-Bonnefoi and Laporte 2002; Cichy et al. 2011; Pichavant et al. 2013; Riker et al. 2015; Fiege et al. 2015). In spite of the increasing interest in reproducing crystallization paths of

multicomponent volatile-bearing systems, our knowledge on the concomitant effect of mixed H₂O+CO₂ fluids on phase relations in alkali-rich basaltic systems is restricted to a more limited number of experimental data (e.g., Freise et al. 2009; Pichavant et al. 2013; 2014; Vetere et al. 2015a). These studies primarily focused on the evolution of phase relations and melt composition across a range of physical and chemical conditions (i.e. P, T, H₂O content), providing information about crystal changes in terms of abundances and size. Previous studies, however, did not directly address changes in magmatic assemblages and crystal stability as a response of fluid flushing which causes local variations in the CO₂ proportion of the magmatic system. The interpretation of textural features of crystals has been, so far, conducted through experimental reproduction of processes of crystal dissolution/resorption or their growth in presence of a pure-H₂O magmatic fluid phase (Logfren 1980; Nelson and Montana 1989; Tsuchiyama 1985; Tsuchiyama and Takahashi 1983; Kawamoto 1992; Kirkpatrick 1981; Hummer and Rutherford 2002). Thus, the influence of volatile components in addition to water on textural and compositional changes in alkali basalts has been generally neglected. This means that mineral reactions in systems undergoing rapid changes of (CO₂-bearing) fluid compositions is still not fully understood, precluding in some cases a proper interpretation of natural samples and of related physical processes during magma ascent.

CO₂ flushing from magmas exsolving gas at depth has been found to play a major role in producing highly explosive eruptions at many basaltic systems such as Etna and Stromboli (cf. Aiuppa et al. 2010a; 2010b; Aiuppa et al., 2016; Allard 2010; Pichavant et al. 2013; Ferlito et al. 2014). In this context, Mt. Etna represents one of the most intriguing cases. The complex plumbing system of Mt. Etna is persistently fed by primitive, volatile-rich magmas that mix with mafic, degassed magmas stored at lower pressure (Armienti et al. 2007; 2013; Ferlito et al. 2008; Viccaro et al. 2010; 2014; 2015; Nicotra and Viccaro 2012a; Corsaro et al. 2013; Mollo et al. 2015). Moreover, published data on primitive glass inclusions in olivine crystals indicate that magmas of Mt. Etna can exsolve a gas phase, rich in CO₂, at pressure higher than 250 MPa (Metrich et al., 2004; Spillert et al., 2006; Collins et al. 2009), which continuously flush the overlying magma

reservoirs, acting as a recurrent trigger mechanism for paroxysmal events (Aiuppa et al., 2007, 2016; Nicotra and Viccaro 2012; Ferlito et al. 2014). This means that a major part of the crystallization occurs in regions of the plumbing system where CO₂ is already exsolved, but in which H₂O activity can change very abruptly as a result of local fluxes of CO₂-rich fluids in magma reservoirs (cf. Aiuppa et al. 2010b; Patanè et al. 2013).

In this study, we tested experimentally the effect of CO₂ flushing in a partially crystallized K-trachybasaltic magma representative of eruptive products from the recent activity of Mt. Etna. We demonstrate that the flushing of CO₂ results in variations of mineral stability and phase relations, which are consistent with observations made in rock samples. The experimental results obtained at 300 and 100 MPa are applied to test the role of CO₂ on mineral textures and melt chemistry during storage in the intermediate (9-6 Km b.s.l.) and shallow (<3 Km b.s.l.) plumbing system of Mt. Etna volcano.

2. Experimental strategy to simulate CO₂ flushing

The experimental strategy applied in this study was chosen to simulate the reaction of a partially crystallized H₂O-bearing magma with a fluid composed of CO₂ and H₂O (with various CO₂ and H₂O molar ratios). Two experimental steps were applied: (1) synthesis of a water-bearing (but water-undersaturated) partially crystallized material at 300 MPa and (2) reaction of this material with a fluid phase ~~to simulate fluid flux~~ at distinct pressure conditions of 300 and 100 MPa. The first step is aimed at reproducing the water-undersaturated basaltic magma ~~prevailing at depth~~ residing at high pressure into the storage system of Mt. Etna prior to CO₂ flushing. The second step simulates a fluid flux across the lower-intermediate plumbing system of Mt. Etna, where the presence of major magma storage zones at depths of 12-9 km and 6-3 km, together with a small reservoir at 1-2 km beneath the summit craters, have been inferred by geophysical studies (Aloisi et al. 2002; Patanè et al. 2006; 2013; Bonaccorso et al. 2011).

2.1 Anhydrous glass synthesis

A natural lava sample ET12_4M from the March 4, 2012 paroxysmal eruption at Mt. Etna was used as starting material (Table 1). This sample is a porphyritic K-trachybasalt ($\text{SiO}_2 = 47.01$ wt.%; Viccaro et al. 2015), which is among the most mafic materials collected at Mt. Etna during the post-2011 eruptive period (see Table 1 for major oxides composition of the sample; cf. Viccaro et al. 2015). This basalt contains 25 vol.% of phenocrysts in the following proportions: 40% clinopyroxene, 30% plagioclase, 15% olivine and 10% titaniferous magnetite. Phenocrysts are generally dispersed in a hyalopilitic groundmass.

The experimental starting material was prepared by crushing the natural lava to a grain size <5 mm. To further improve the homogeneity, an agate mortar was used to produce more fine-grained powder. The sample was melted for 3 hours in a Pt-crucible placed in a furnace at 1600°C and 1 atm. Then, the melt was quickly quenched to glass by quenching it directly on a brass plate. To improve the homogeneity of the mixture, the glass was grinded again in an agate mortar and melted for 2 hours at the same conditions. The major element composition and homogeneity of the final quenched basaltic anhydrous glass were examined by a Cameca SX 100 electron microprobe at the Institut of Mineralogy of the Leibniz Universität Hannover, Germany (Table 1). Analytical procedures for the Electron Microprobe Analysis (EMPA) are provided in Section 3.3. The glass was crushed and divided in two fractions with diameter of <200 μm and $200\text{-}500$ μm . Before loading into experimental capsules, the two grain-size powders were mixed in a volume ratio of 1:1 to minimize the free volume between grains and hence, to reduce the incorporation of atmospheric water or nitrogen into the charge (Vetere et al. 2015a and references therein). This procedure ensures a more uniform distribution of fluids and avoids the incorporation of absorbed water in the sample container.

2.2 First step experiment: sample preparation and starting material for the flushing experiments

The glass powder prepared at 1 atm was first used to synthesize a hydrous glass containing 1 wt.% H₂O. A 40 mm long Au₈₀Pd₂₀-tube, with a diameter of 5.0-5.4 mm, was used to perform the experiments. ~~After annealing at 950°C, the capsule was prepared by loading~~ The capsule was annealed at 950°C and prepared for the synthesis of the hydrous glass by loading ≈1.0 g of glass powder and 1 wt.% of deionized water ~~for the synthesis of the hydrous glass~~. The capsule was ~~Capsules were~~ filled in several steps to achieve homogenous initial distribution of water and glass. Water was added step by step to dry glass powders and the charge was compressed after each addition of water by using a steel piston. Finally, the capsule was welded and checked for leakage of water by annealing at 110°C for about 2 hours. No water loss was detected by re-weighing the capsule. This capsule was used to synthesize a water-bearing glass at superliquidus conditions (1250°C, 300 MPa) in an internally heated pressure vessel (IHPV). The superliquidus conditions at 1250 °C at 300 MPa are confirmed using MELTS software and taking the average bulk rock composition of the March 2012 lavas of Mt. Etna as melt composition. After quench, the glass was analyzed for its water concentration by KFT (see below) and the remaining part was used again for step 1 experiment aimed at producing the starting material for CO₂-flushing experiments. The choice to hydrate the glass with only 1 wt.% of water relies on the intention to produce a starting material containing plagioclase at high pressure conditions. Such a choice also accounts for results of the hygrometer of Putirka (2008) applied on plagioclase cores from sample ET12_4M, which suggests an early crystallization of plagioclase at depth of 300 MPa, at ~1100°C with melt water content between 0.5 and 1.2 wt.%. The amount of added water also ensures that the melt is volatile-undersaturated (fluid-absent conditions) at the conditions of step 1 experiment (300 MPa, 1080°C).

To describe accurately textures obtained from the reaction of an assemblage (melt + mineral) in disequilibrium with fluids (simulating the fluid flux, see second step experiments), the approach of step 1 experiment was chosen to obtain particularly large crystals in the synthesis of the melt + mineral assemblage (step 1). The sample was prepared as described above for the synthesis of the

water-bearing glass and brought to superliquidus conditions at 1250°C and 300 MPa for approximately one hour in an internally heated pressure vessel (IHPV). Subsequently, nucleation and crystallization processes were induced by lowering the temperature from liquidus conditions to 1080°C with a cooling rate of 20°C/min. Finally, 25 thermal cycles of two hours each with a temperature oscillating between 1060 and 1100 °C were applied. Pressure was kept constant at 300 MPa by automatic compensation. Before quenching, the temperature was set to the mean temperature (1080°C) for 20 minutes.

Crystallization under oscillating temperatures was done because this procedure decreases the number of crystals and enhances the size of crystals if the selected temperature interval is below the liquidus (cf. Hintzmann and Muller-Vogt 1969; Mills et al. 2011; Mills and Glazner 2013; Erdmann and Koepke 2016). When temperature is increasing (1060 to 1100 °C) crystals initially present at low temperature are partially dissolving and only the large crystals are expected to remain in the charge. When temperature is decreasing (1100 to 1060 °C) the crystallization is expected to occur mainly in the interface between the pre-existing crystals and the melt. The product obtained after the synthesis shows ~~indeed~~ crystals of clinopyroxene and plagioclase that are larger than 1 mm (Fig. 1). This product, labeled S0 in the following study, was used as starting material for the subsequent experiments in which a H₂O+CO₂ fluid mixture was added.

2.3 Second step experiments: CO₂ flushing

Two set of experiments were performed at two different pressures of 300 MPa and 100 MPa in order to reproduce CO₂-flushing at different levels of the Etnean plumbing system. Slices (14-20 mg) of the starting materials S0 were encapsulated in Au₈₀Pd₂₀-tubes together with deionized water and silver oxalate (Ag₂C₂O₄), which was used as source of CO₂. The ratio between the solid material S0 and the fluid phase (H₂O+CO₂) is given in Table 2. Water and silver oxalate were loaded into the capsules with different proportions to establish different mole fractions of CO₂ in the fluid composition at the onset of step 2 runs (XCO₂^{fl} from 0.24 to 0.94; Table 2). Capsules were

weighted after loading of each component and the welding; they were finally checked for leakage by annealing in oven for at least 1 hours at 110°C. For each set of experiments, three capsules were run simultaneously in order to evaluate the post-run compositional and textural changes for distinct fluid composition at exactly the same pressure and temperature conditions. The duration of each run was about 24 hours.

The P-T conditions selected for the fluid-bearing experiments (1080°C, 300 and 100 MPa) are consistent with those of the lower-intermediate plumbing system of Mt. Etna (Aloisi et al. 2002; Patanè et al. 2006; 2013; Bonaccorso et al. 2011). However, it must be noted that the experiments were performed at 1080°C, a temperature slightly lower than those generally assumed for Etnean K-trachybasaltic magmas at intratelluric condition (cf. Tanguy and Clocchiatti 1984). This slightly lower temperature enhances the crystallization of all mineral phases observed in the natural samples and leads to an increase of the crystal mean size.

3. Experimental and analytical methods

3.1 Internally heated pressure vessel (IHPV)

The IHPV apparatus used in this study is described in detail by Berndt et al. (2002). The temperature was measured by four unsheathed S-type thermocouples and an Eurotherm software was used to control temperature cycling and to record the measured temperature along the whole experimental run time. Precision of temperature of each thermocouple was $\pm 10^\circ\text{C}$. Argon is the pressurizing medium and pressure was monitored by digital pressure transducers with an uncertainty of about 1 MPa. The variation of pressure during the experiments was < 5 MPa. Experiments were performed at the intrinsic hydrogen fugacity of the vessel. Under intrinsic conditions in the IHPV, the oxygen fugacity in capsules containing H₂O-saturated melts (pure H₂O fluid) was found to be close to the MnO-Mn₃O₄ or NNO + 3.7 buffer (Berndt et al. 2002). It must be taken into account that, with increasing amount of loaded CO₂, the oxygen fugacity decreases due to the lowering of water activity, i.e., an increase in $X_{\text{CO}_2}^{\text{fl}}$ from 0.1 to 0.9 decreases the f_{O_2}

by roughly two logarithmic units (e.g., Botcharnikov et al. 2005, Vetere et al. 2014). The redox conditions prevailing within capsules were also determined on post-run products using the oxygen barometer of Ishibashi (2013), which is based on the spinel-melt equilibria (see analyses of glass and spinel in the electronic supplementary material ESM). The calculated $\log f\text{O}_2$ varies between 10^{-6} to $10^{-7.3}$ bars, corresponding to a $f\text{O}_2$ ranging between NNO +2.9 and NNO +1.7 log units (Table 2). At the end of each run, samples were quickly quenched isobarically by dropping the capsule down into the cold part of the vessel, in order to avoid any non-equilibrium quench effects (rapid quench technique; estimated cooling rate was about $150^\circ\text{C}/\text{s}$; Berndt et al. 2002).

3.2 Measurements of H_2O content in initial hydrous glasses

Karl-Fischer titration (KFT) method was adopted for the determination of the water concentrations in quenched initial glasses that were synthesized at superliquidus conditions and used for the first step experiment. Water is extracted by heating the sample up to temperature of about 1300°C and the released water is measured by coulometric titration. The coulometer used in this study is a Mitsubishi CA100. The benefit of the KFT method is that only small amounts of glass are required to get reliable analyses. In this study, about 50-100 mg of glass were required for water content of 1 wt.%. The extraction of water from the glass or melt with this technique can be incomplete in silica-rich glasses (Behrens 1995). Typically, about 0.10 wt.% of non-extracted H_2O was found in samples containing initially more than 1.5 wt.% H_2O (Behrens 1995; Leschik et al. 2004), implying that the water contents obtained with KFT methods may have to be corrected for values of residual water content. As the water diffusivity is much faster in silica-poor melts than in silica-rich melts (Behrens 1995; Behrens et al. 2004), the extraction of water should be greatly enhanced in the basaltic melts under investigation. Hence, the 1.1 wt.% H_2O measured with KFT for ET12_M4 glasses can be assumed as representative of the real water content of the sample, and corrections for non-extracted water were not required. Considering that, after the cycling experiments the amount of crystallized phases [plagioclase, clinopyroxene and Fe-Ti oxide are 12.0,

22.9 and 3.8 area % respectively, calculated via image analyses as described in Vetere et al. (2015b)], mass balance calculations allow to infer the water content in the residual melt to a value of ≈ 1.5 wt.%. To test the accuracy of this value and provide a more accurate estimate of the initial water content for the equilibrium run S0, we used the plagioclase-liquid hygrometer of Waters and Lange (2015), which is based on the crystal-liquid exchange reaction between the albite and anorthite component and is applicable to a wide range of magmatic composition from basalts to rhyolites and alkaline magmas. Application of the hygrometer, using the temperature of 1080°C with the plagioclase (An58) and liquid composition of S0, results in a dissolved water content of 1.6 ± 0.35 wt.%, a value close to the previous estimate.

3.3 Determination of sample fluid compositions after experiments

The mole fractions of H₂O and CO₂ in the fluid phase after experiments were calculated through mass balance using the initial amounts of loaded volatiles, rock powders and the estimated concentrations of volatiles retained in the melt after each experimental run. The H₂O and CO₂ concentrations in the melt and the related composition of the fluid were determined using the MagmaSat software based on the thermodynamic model of Ghiorso and Gualda (2015), which allows us to calculate the saturation conditions for mixed H₂O-CO₂ fluids in natural silicate melt. In all the samples, the ~~H₂O-CO₂ degassing behavior~~ H₂O and CO₂ partitioning between melt and fluid was modeled starting from the average composition of the run product glasses. The modelled H₂O and CO₂ contents in the melts are in the range 3.06-0.73 wt.% H₂O and 0.25-0.20 wt.% CO₂ for experiments performed at 300 MPa and 2.53-0.54 wt.% H₂O and 0.07-0.03 wt.% CO₂ at 100 MPa (Table 2). Such concentrations are in the same range than those determined from melt inclusion analyses from other recent eruptions of Mt. Etna (Métrich et al. 2004; Spilliaert et al. 2006a; Collins et al. 2009).

3.4 Electron Microprobe Analysis (EMPA)

Major element compositions of the starting dry glass and the experimental products, composed of minerals and glass, were analyzed by a Cameca SX-100 electron microprobe at the Institute of Mineralogy of the Leibniz Universität Hannover, using 15 kV as the acceleration voltage. Conditions of measurement during glass analyses were 4 nA beam current and 20 μm diameter of electron beam. Following the procedure used at Hannover for the analysis of experimental charges containing hydrous basaltic glasses and minerals (e.g., Husen et al., 2016), peak counting times for glasses vary from 4 seconds for Na and K, to 8 seconds for the other elements. The analyses on minerals were conducted with a 15 nA beam current and a focused electron beam. Peak counting time was 5 seconds for Na and K, and 10 seconds for the other elements. Standard glasses and crystals were used for calibration. The composition of the starting dry glass is an average of 6 analyses. The average dry glass composition and related standard deviation is given in Table 1. Multiple point measurements were made for mineral phases and glasses of the experimental products to check the sample homogeneity and to reduce possible analytical errors. For some of the largest plagioclase crystals (~ 1 mm size), core-to-rim profiles were measured through single grains to determine changes in the chemical composition. Microprobe data for post-run minerals and glasses are synthesized in Table 3. The whole dataset is available as Electronic Supplementary Material (ESM hereafter).

4. Experimental Results

4.1 Mineral assemblage and composition of the hydrated starting material (S_0)

Hydrated products resulting from crystallization at 300 MPa (sample S_0 in Figure 1) consist of glass (~ 61 vol.%) and a mineral assemblage constituted by plagioclase (~ 12 vol.%) and clinopyroxene (~ 23 vol.%). Abundant and relatively small (20-150 μm in size) Fe-Ti oxides, mainly titaniferous magnetite, are present in proportion of ~ 4 vol.% of the sample (Fig. 1). The glass compositions, reported in Table 3, fall in the field of the basaltic trachyandesite ($\text{SiO}_2 = 52\text{-}53$ wt.%; $\text{Na}_2\text{O}+\text{K}_2\text{O} = 8.2\text{-}8.6$ wt.%). As a whole, the observed mineral assemblage resembles that of

the natural lava samples from Mt. Etna 2012 eruptions, with the exception of the lack of olivine crystals. The absence of olivine in S0 may be related to the rather oxidizing experimental conditions and to the effect of oxygen fugacity on the stability field of olivine. An increase of oxygen fugacity reduces the stability field of olivine (e.g., Roeder and Emslie 1970; Carmichael and Ghiorso 1990; Berndt et al. 2005; Feig et al., 2010).. Clinopyroxene is the most abundant mineral phase with size from 200 μm to about ~ 1 mm and with a diopsidic composition ($\text{Wo}_{47-50}\text{En}_{30-38}\text{Fs}_{14-21}$). The Mg# [atomic ratio $\text{Mg}/(\text{Fe}+\text{Mg})$] varies between 77 and 88 (Fig. 2; electronic supplementary material, ESM hereafter). Clinopyroxene crystals display hollow cores and euhedral rims that indicate skeletal crystal growth possibly induced by the rapid initial cooling of the step 1 run. Plagioclase occurs as euhedral crystals up to 1 mm in size and is labradoritic in composition (An_{55-64} ; Fig. 2; ESM). The chemical zoning of plagioclase is characterized by oscillations of the anorthite (An) content in a range of ~ 10 mol%. This feature is consistent with crystallization of plagioclase in a system with temperatures oscillating in a range of 40°C (Singer et al. 1995; Couch et al. 2001). It is worth noting that the average An content of plagioclase in the experimental sample is significantly lower than that of natural products of Mt. Etna, which typically covers a wider range from bytownite to labradorite, with subordinate, rare anorthite crystals (Viccaro et al. 2010; 2015; 2016). Textural relations between minerals show that most of the plagioclase nucleated when clinopyroxene and oxides were already formed, indicating that the growth of clinopyroxene and Fe-Ti oxides was faster than that of plagioclase (cf. Hammer and Rutherford 2002; Fig. 1).

4.2 Mineral assemblage and mineral composition after CO_2 - H_2O flushing

Textural characteristics of the sample S0 after fluid flushing at 1080°C are shown in Figure 3 and Figure 4 for experiments performed at 300 MPa and 100 MPa, respectively. At each pressure three experiments with different initial XCO_2 of the fluid phase were performed. Since the liquidus temperature of tectosilicates is strongly depended on the water activity (i.e., the liquidus

temperature decreases with increasing water activity), plagioclase is found only in sample where XCO_2^{fl} is high, as expected (Fig. 3e-f and Fig. 4c-f).

The high pressure experiments at 300 MPa produced a mineral assemblage with clinopyroxene and titaniferous magnetite for $XCO_2^{fl} = 0.4$ (sample 300_S2; Fig. 3a-b) and $XCO_2^{fl} = 0.7$ (sample 300_S3; Fig. 3c-d). At 300MPa and $XCO_2^{fl} = 0.4$ we observed relicts of clinopyroxene clearly affected by pervasive dissolution, which have compositions $Wo_{47-50}En_{33-38}Fs_{15-20}$ and average Mg# 85 (see Table 3; ESM). The crystal size is in the order of 300 to 400 μm (Fig. 3a-b) and is smaller than in the starting material S0. The composition of clinopyroxene is more evolved at $XCO_2^{fl} = 0.7$ ($Wo_{45-50}En_{32-37}Fs_{15-20}$; average Mg#81; Table 3; ESM), moreover, the maximum size is $\sim 100 \mu m$ and crystals tend to have a more euhedral habitus than those observed at lower XCO_2 Fig. 3c-d). Oxides are 5-60 μm in size and constitute $\sim 5\%$ of the volume of the phenocryst phases; their compositions are comparable in both, At 300 MPa and $XCO_2^{fl} = 0.9$ (sample 300_S4) clinopyroxene and Fe-Ti oxides coexist with plagioclase (Fig. 3e-f). Plagioclase forms sub-euhedral crystals up to $\sim 500 \mu m$ in size, commonly characterized by dissolution textures along their edges (compare Fig. 1 and Fig. 3f). Plagioclase composition is labradoritic (An_{57-65}) and rather similar to that in S0 (Table 3; ESM; Fig. 2). Clinopyroxene is euhedral to sub-euhedral with composition $Wo_{46-49}En_{30-39}Fs_{14-22}$ and a size of $\sim 300 \mu m$. In contrast to plagioclase showing dissolution textures (Fig. 3f), clinopyroxene has rims usually marked by more Ca and Mg-rich envelopes (Mg# 87-89) enclosing cores. This composition more Mg-rich than that in S0 (Mg# 76-82; see ESM; Fig. 3e-f). The crystallinity of the products at 300 MPa increases progressively from ~ 10 vol.% in sample 300_S2 (high H_2O -low CO_2) to ~ 30 vol.% in 300_S4 (low H_2O -high CO_2). The higher crystallinity and lower crystal size of 300_S4 relative to S0 results in an increase in crystal number density. This feature can be explained by the lower melt water content in 300_S4 (0.74 wt.% H_2O) when compared with 300_S2 (1.60 wt.% H_2O) (Bugger and Hummer 2010; Riker et al. 2015).

At 100 MPa and $XCO_2^{fl} = 0.2$ (i.e. sample 100_S1), the product is only composed of glass ($SiO_2 = 48$ wt.%) and zoned clinopyroxene ($Wo_{47-50}En_{34-39}Fs_{13-17}$; average Mg# 0.91; see ESM; Fig.

2; Fig. 4a-b). The mineral assemblage changes to clinopyroxene, plagioclase and titaniferous magnetite at higher proportion of CO₂ in the fluid (i.e. 100_S2 and 100_S4; Fig. 4). For XCO₂^{fl} = 0.2 clinopyroxene is euhedral to subhedral with some evidences of dissolution at the core. The shape of the clinopyroxenes is similar in the experiments at XCO₂^{fl} = 0.2 and XCO₂^{fl} = 0.5 (i.e. 100_S1 and 100_S2). However, the amount of clinopyroxene is clearly lower than in S0, indicating that dissolution and recrystallization probably occurred in these two experiments. At the highest XCO₂ (sample 100_S4), clinopyroxene shows skeletal textures similar to those of S0, though crystals greatly differ in size that is much smaller for the 100_S4 crystals (~200 μm; Fig. 4e-f); textural observations do not help to clarify if this mineral grew or dissolved. Despite the variations in crystal textures, the abundance and composition of clinopyroxene correlate with the CO₂ concentrations in the fluid. As the XCO₂^{fl} of the system increases, the proportion of clinopyroxene becomes higher, whereas the average Mg# decreases from 0.91 (100_S1) to 0.84 (100_S4; Fig. 2; see ESM). When present, plagioclase occurs as 200 to 300 μm-large oscillatory-zoned crystals with composition ranging from An₅₃ to An₆₅ (Table 3; ESM). Observations under optical microscope and BSE images indicate that the size of plagioclases is much lower compared with the starting material S0 and, on average, it decreases by a factor of 2 in both the 300 MPa and 100 MPa experiments. Most plagioclase crystals have elongated euhedral habitus, but there are also crystals with subhedral to anhedral habitus, characteristic for dissolution textures (Fig. 4). Thus, textural observations indicate that plagioclase dissolved in all experiments at 100 MPa.

4.3 Composition of the experimental glasses

Major element composition of glasses record progressive melt evolution as a response of increasing CO₂ content in both sets of experiments (see ESM; Fig. 5). At a given pressure, K₂O and Na₂O become more concentrated in the melt with increasing XCO₂, while concentrations of MgO, CaO and TiO₂ decrease (Fig. 5). The comparison between the glass composition of sample S0 and that of the samples flushed with CO₂ is helpful to test the textural observations indicating

dissolution or growth of the solid phases. Since K_2O behaves almost as an incompatible element, K_2O concentration in the residual glasses is a good proxy for tracing the crystallinity. Except for the experiment at 100MPa and 0.9 XCO_2^{fl} (sample 100_S4), all charges record a significant decrease of K_2O with respect to sample S0, indicating a decreasing bulk crystal content with increasing XCO_2 (Fig.5). For sample 100_S4, the K_2O glass concentration is very close to that of S0, a feature that reflects a crystal/liquid proportion which is similar to that of the starting material.

A detailed analysis of the compositional variation of the elements other than K_2O provides additional information on crystal growth or crystal dissolution during flushing experiments (Fig. 5). The Na_2O , Al_2O_3 , CaO and MgO composition of glasses in samples 300_S2, and 100_S1 compared to S0 indicate that both clinopyroxene and plagioclase dissolved in these experiments at low XCO_2 . The experiment 300_S3 (300 MPa, 0.7 XCO_2^{fl}) contains only clinopyroxene and no plagioclase, but the Na_2O content of the glass in this experiment is slightly higher than that of the S0 (Fig. 5). This behavior can only be explained if a Na-poor phase (i.e., clinopyroxene) is crystallizing, as confirmed by the textural observation. The glass composition of sample 300_S4 (0.9 XCO_2^{fl}), which has lower MgO concentrations and higher Na_2O and Al_2O_3 than S0, also implies that clinopyroxene is crystallizing and plagioclase is dissolving in this experiment. The glass composition of the experiment 100_S2 (0.5 XCO_2^{fl}) can only be explained if both phases are dissolving. In this case, evidence for plagioclase dissolution is given by textural observations, but the higher MgO content of the glass also indicates that clinopyroxene is slightly dissolving (Fig. 5). For the sample 100_S4 (0.9 XCO_2^{fl}), K_2O indicates that the crystallinity is similar to S0. However, the slightly higher Na_2O content of the glass in 100_S4 (at similar CaO , MgO and Al_2O_3 concentrations; Fig. 5) indicates that a small proportion of clinopyroxene is crystallizing and that a small proportion of plagioclase is dissolving. The evolution of most Fe-Ti oxides can be reconciled with crystallization or dissolution processes of the two minerals, i.e. clinopyroxene and plagioclase. However, FeO has a different behavior. The concentration in all glasses is in the same range (7.0 to 7.5 wt.% FeO) and is higher than that of S0 (Fig. 5). This higher FeO content is explained by the

lower proportion of Fe-Ti oxides (dissolution) in the step 2 experiments, a feature also noted from textural observations. The dissolution of oxides is likely due to a slightly different oxygen fugacity in the S0 and in the step 2 runs (see Table 2).

5. Discussion

5.1 Textural and compositional observations on minerals

The comparison of the starting material S0 with the experiments performed at 300 and 100 MPa at various $X_{CO_2}^{fl}$ gives us a direct link to understand the role of CO_2 on the phase stability of basaltic systems enriched in carbon dioxide, such as Mt. Etna. In particular, we observed that the high a_{H_2O} in the system during crystallization of Etnean basalts at 300 MPa caused complete dissolution of plagioclase in samples 300_S2 (3.06 wt.% H_2O in the melt) and 300_S3 (1.90 wt.% H_2O in the melt). Conversely, flushing the system with fluids with high CO_2 proportions at high pressure (run 300_S4, 0.73 wt.% H_2O in the melt), strongly destabilizes plagioclase, which develops dissolution textures despite the water content of the system is significantly reduced with respect to S0 (Fig. 1 and Fig. 3e-f). At 100 MPa plagioclase crystals are present in samples 100_S2 and 100_S4 for melt water contents between 1.78 and 0.54wt. %. These crystals have subhedral habitus with minor evidence of dissolution surfaces in both 100_S2 and 100_S4 samples (Fig. 4c-f).. Even more interesting is the fact that the amount of water in melts of the plagioclase-bearing charges 300_S4 and 100_S4 is significantly lower than in the starting material S0 (see Table 2), a condition that should promote the plagioclase stability and enhance crystal growth according to a number of experimental studies (e.g., Housh and Luhr 1991; Lange et al. 2009; Almeev et al. 2012). Nevertheless we observed that plagioclase is dissolving in these two experiments.

Different proportions of H_2O and CO_2 in the experimental charges also produce major variations of textures of clinopyroxene that are ubiquitous in all the samples. Textures of clinopyroxene crystals vary at increasing $X_{CO_2}^{fl}$, with different behavior depending on pressure. In the high pressure experiments the clinopyroxene is destabilized for high melt water concentration

(3.0 wt.% H₂O, sample 300_S2; see Table 2), but its stability gradually expands at increasing CO₂ in the fluid phase; under these conditions clinopyroxene crystals develop Ca- and Mg-rich growth zones towards the rim (Fig. 3e-f). Low-pressure charges at high water concentration in the melt and low XCO₂^{fl} display euhedral grains of clinopyroxene (sample 100_S1, 2.5 wt.% H₂O), whereas crystals with hollow cores and anhedral rims are characteristic for charges flushed with a fluid with high CO₂ proportions (sample 100_S4, 0.54 wt.% H₂O). However, comparison between the starting material S0 and experimental samples of run 2 indicate increasing modal proportion of clinopyroxene for elevated proportion of CO₂ during both the high and low pressure experiments.

Despite the evidence of textural changes for plagioclase and clinopyroxene, the incorporation of large amount of CO₂ in the starting material does not produce significant compositional changes on the entire phase assemblage that preserve compositions very close to that of S0 (Fig. 2). As a whole, we observed that the effect of changing CO₂ proportions in basaltic melts is small on clinopyroxene Mg# at 300 MPa (Δ Mg# ~2%). Clinopyroxene records more prominent chemical changes at 100 MPa; the Mg# correlates negatively with XCO₂, shifting from 0.84 for XCO₂^{fl}=0.9 to 0.91 for XCO₂^{fl}=0.2. Plagioclase behaves similarly at 100 MPa, with the average An content of plagioclase increasing slightly from An₅₈ at XCO₂^{fl}=0.9 to An₆₀ at XCO₂^{fl}=0.5. However, the chemical variation of plagioclase may not be representative, given that analytical errors are on the order of 2 mol% An.

On the whole, the mineral chemistry of experimental products is similar to products emitted at Mt. Etna both in historic and recent eruptions. With the exception of the clinopyroxene crystals obtained very low XCO₂, the composition of the experimental clinopyroxene is in the range of compositions of the natural samples, which falls in the fields of diopside-salite and augite, and has average Mg# between 0.79 and 0.83 (Giuffrida and Viccaro, 2017). Similar observations can be done for plagioclase: the experimental phases fit the compositional range observed for plagioclase crystals found in Etnean natural samples [An₄₇₋₉₁, with frequency peaks at the labradoritic compositions for crystals of the historic and recent activity (Viccaro et al., 2010; 2016)].

5.2 Reaction of the mineralogical assemblage on CO₂ flushing

The isobaric and isothermal experimental series presented in this paper simulate the reaction of a magma as a result of changing H₂O and CO₂ proportions in the volatile mixture only (constant temperature and pressure). The classical phase equilibria studies in mafic systems in which one bulk composition is in equilibrium with a H₂O-CO₂-bearing fluid phase all indicate that the phase proportions of both plagioclase and clinopyroxene should decrease with increasing water activity at fixed temperature and pressure (e.g., Feig et al. 2006; Pichavant and Mac Donald 2007; Almeev et al. 2013). The analysis of previous studies shows that the same general observation can be done in pure H₂O-bearing systems (no CO₂): reduction of the water concentration in the melt promotes the plagioclase and clinopyroxene stability and enhances crystallization (e.g., Moore and Carmichael 1978; Blundy and Cashman 2001; Berndt et al. 2005; Almeev et al. 2012). Our experiments indicate (1) that the effect of H₂O on the stability and mineral proportion of plagioclase is much more pronounced than that of H₂O on clinopyroxene, a result that is in agreement with past experimental studies and (2) that clinopyroxene is crystallizing and plagioclase is dissolving in some experiments. This unexpected last observation cannot be reconciled with the previous phase equilibria studies and needs a detailed discussion.

Crystallization of clinopyroxene and dissolution of plagioclase was observed in two experiments at 300 MPa and one experiment at 100 MPa. In two of these experiments (run products at very high XCO₂), the water content of the melt is clearly lower than the initial water content (estimated to be 1.6 wt% H₂O; Table 2). The third experiment at 300 MPa has approximately the same H₂O content of the melt than the starting material prepared at the same pressure (~1.9 wt% H₂O). Compared with the general results obtained in pure H₂O-bearing systems, the crystallization of clinopyroxene in the systems with lower H₂O content of the melt than the starting material can be expected. Thus, the behavior of clinopyroxene in the flushing experiments is consistent with previous experiments but the dissolution of plagioclase is problematic and difficult to explain. The experimental approach used in our two step experiments implies that a CO₂-free assemblage (first

step) is reacting with a H₂O-CO₂-bearing fluid (second step). Thus, at high XCO₂, H₂O is released from the melt and CO₂ is incorporated into the melt phase. Considering that the decrease of water content only is not expected to cause a dissolution of plagioclase (see above), another parameter must be taken into account, especially in the 300 MPa experiments because both steps (synthesis of the starting material and flushing experiment) were conducted at the same pressure. In addition to changing melt water content, three explanations can be proposed for the plagioclase dissolution observed in the 300 MPa experiments: disequilibrium in the S0 and/or in step 2 experiments, oxygen fugacity and the CO₂ content of melt.

Disequilibrium due to crystallization kinetics in S0 run: The shape of the minerals observed in the S0 experiments (Fig. 1) is not that expected for minerals in textural equilibrium with a melt phase. Thus, it may be possible that equilibrium was not attained in the S0 experiment. The shape and the large size of the minerals in the S0 run is related to the temperature path of the experiment, which started from an initial temperature of 1250°C at conditions above the liquidus. At this stage a homogeneous melt phase was formed and nucleation within a homogeneous melt is known to be difficult, in contrast to experiments starting directly from a glass powder. Thus, with a cooling rate of 20°C/min, the growth rate of the few minerals that nucleated is expected to be fast, probably leading to minerals with a skeletal shape. The subsequent temperature cycling explains the compositional variations of the large minerals. However, a detailed analysis of Figure 1 indicates that the evidence of a skeletal shape is observed in the internal part of the crystals, but the outer part of the mineral phases is in textural equilibrium (the typical crystalline orientations of plagioclase and clinopyroxene can be recognized). Considering the sluggish nature of plagioclase, it is possible that equilibrium proportions of plagioclase were not reached in the S0 experiments (~ 50 hours). However, in this case, unexpected crystallization of plagioclase would occur in the step 2 experiments, but not dissolution as observed in this study. Thus, problems related to the kinetics of plagioclase growth in S0 runs cannot explain the experimental observations.

Diffusivity of volatiles in step 2 runs: The step 2 experiments were conducted by equilibrating a fluid phase with a 14-20 mg piece of partially crystalline sample. Since H₂O can diffuse faster than CO₂ in silicate melts (e.g., Zhang and Ni, 2010) the dissolution of plagioclase could be explained by disequilibrium between the volatile concentration in the melt and the fluid in the first stages of the experiment. In this case, the water activity in the central part of the samples may be higher than expected leading to dissolution of plagioclase, but dissolution textures should not be observed in rim of the samples. This contrasting behavior in the rim and the core of the samples was not observed. In addition, the chips used for the step 2 experiments are small and equilibrium is expected to be reached after 24 hours in depolymerized basaltic melts. However, considering the sluggish reaction of plagioclase, this explanation cannot be definitely excluded.

Oxygen fugacity: In IHPVs, the decrease in water activity is accompanied by a decrease in oxygen fugacity, as described by Scaillet et al. (1992) and Botcharnikov et al. (2005). However, phase equilibria in mafic systems at relatively low water contents do not indicate that the plagioclase stability is strongly affected by changing redox conditions in the fO_2 range explored in this study. At water activity close to unity, the liquidus temperature of plagioclase may be slightly depressed with decreasing fO_2 in trachytic or granodioritic systems (e.g. Dall'Agnol et al. 1999; Martel et al. 2013). Results obtained in basaltic and granodioritic systems at water activities below 0.5, which may be more relevant for comparison with this study, do not show a strong influence of oxygen fugacity on the beginning of crystallization of plagioclase (e.g. Dall'Agnol et al. 1999; Berndt et al. 2005; Botcharnikov et al. 2008) and of clinopyroxene (Botcharnikov et al. 2008). However, even if strong effects were not detected within 50 °C intervals (usually the temperature intervals for the phase equilibria were 50 °C) oxygen fugacity is expected to cause structural changes in the melt by changes of the Fe²⁺/Fe³⁺ ratio, which should at least affect slightly the stability of clinopyroxene, magnetite, and plagioclase.

Except for the results presented in this study, there is no experimental data allowing us to compare the stability of plagioclase at constant melt H₂O content between H₂O-CO₂-bearing

systems and H₂O-bearing systems. Since changes of phase stabilities due to variations of f_{O_2} only may not be sufficient to explain the experimental observations, our results indicate that the incorporation of small amount of CO₂ in silicate melts as carbonate species influences significantly plagioclase stability (e.g., preferential bonding of Ca with carbonates in the melt phase can affect plagioclase stability). This hypothesis is consistent with the differences observed at 100 and 300 MPa. Our experimental results indicate that dissolution of plagioclase is more pronounced at 300 MPa than at 100 MPa, which may be related to the higher concentration of dissolved CO₂-bearing species at high pressure (e.g., Shishkina et al. 2014b; Vetere et al. 2014). Considering the H₂O and CO₂ solubility data in silicate melts from Etna (Shishkina et al. 2014b), approximately 3000 ± 500 ppm CO₂ should be incorporated in Etna basalts at 300 MPa and at high XCO₂. In our experimental melts, this concentration may reach 5000 ppm or more, considering that the melts obtained at high XCO₂ were more alkali-rich than the starting melts and that CO₂ solubility is increasing with increasing alkalis (Vetere et al. 2014). Since Fe²⁺/FeO_{tot} ratio is directly proportional to the amount of CO₂ dissolved in melts (Vetere et al. 2014), f_{O_2} changes to lower values (or more reduced conditions) may also increase the amount of dissolved CO₂. However, if our hypothesis is correct, the strong effect of such low CO₂ concentrations on the plagioclase stability is surprising and may be important to understand the effects of CO₂ fluxes in magmatic systems.

The most reliable explanation for the textural observations made in this study is a combination of structural effects resulting from CO₂ incorporation and from changes of activities of the individual components due the different effects of volatiles (H₂O and oxygen fugacities) on the stability of solid phases (e.g. H₂O has a stronger effect on the stability of plagioclase than on the stability of clinopyroxene). However, although not detected in the experimental products, kinetic effects due to different diffusivities of H₂O- and CO₂-bearing species in the basaltic melts cannot be fully excluded. However, additional systematic tests should be performed to confirm the results of our pilot experiments.

6. Implications and conclusions

Empirical investigations aimed at reproducing the interaction between silicate melts and volatile species, where the fluid is realistically multicomponent, i.e. $\text{H}_2\text{O}+\text{CO}_2$, are crucial for interpreting pre-eruptive history of magmas that are largely enriched in CO_2 , such as those of Mt. Etna. Our experiments on Etnean K-trachybasalts directly simulate processes of CO_2 -flushing at distinct sections of the plumbing system, providing new insights for interpreting the range of crystal textures observed in natural samples.

Although compositions of the experimental mineral phases do not significantly change with CO_2 , we have evidence that plagioclase and clinopyroxene react differently as a consequence of the addition of significant amounts of CO_2 . Under elevated CO_2 proportion with respect to water, plagioclase crystals may experience severe dissolution at 300 MPa, whereas the destabilization of plagioclase is less pronounced at 100 MPa. Clinopyroxene textures change differently during the high and low pressure experiments of flushing. Clinopyroxene stability expands and crystals display growth textures at 300 MPa and high X_{CO_2} ; in contrast, clinopyroxene growth is much less pronounced at low pressure for comparable volatile concentration.

Because CO_2 may have a significant influence on magma crystallinity, the effects of CO_2 -flushing on products from the recent activity of Mt. Etna cannot be neglected for a proper interpretation of pre-eruptive dynamics. In Etna basalts, the presence of plagioclases characterized by cores with dissolution/resorption textures, such as coarse-sieve and patchy textures, is common (Viccaro et al. 2010; 2014; 2015; 2016; Giuffrida and Viccaro 2017 Fig.7). Moreover, the rims of plagioclase are often affected by single or multiple sieve textures (Fig.7). Most of the augitic clinopyroxenes that were found in lava rocks from the post 2011 paroxysmal activity (e.g. eruptions of March 04, 2012, and April 18, 2013; cf. Viccaro et al. 2014, 2015; Giuffrida and Viccaro 2017) also display destabilization along the rim, sometimes evolving to pervasive disequilibrium features similar to sieve textures (Fig.7). The development of disequilibrium features at the crystal rims has been often attributed to processes of recharge of the residing system by more basic magma, whereas

decompression of water-undersaturated magmas has been thought to be the main process controlling the destabilization of crystal cores (Viccaro et al. 2010, 2014; Giuffrida and Viccaro, 2017). Experimental results presented in this paper demonstrate that the reaction of crystal-bearing magmas with CO₂-rich fluids may also be responsible for the range of disequilibrium textures observed in the crystal cores and rims.

Exploring the degassing path of Etnean magmas variably enriched in H₂O and CO₂, various authors concur on a CO₂ exsolution depth >400 MPa, i.e. a depth greater than the depth of the plagioclase crystallization threshold which is located at ~12 km, corresponding to ~340 MPa (Viccaro et al. 2010). Conversely, water is kept almost entirely dissolved in the melt up to ~5.5-7 km (~155-200 MPa). This means that, at the highest pressure investigated by our experiments, i.e. 300 MPa, the system is already volatile-saturated. Although the water concentration in the melt is probably enough to produce plagioclase dissolution/resorption during magma decompression below depths of 5.5–7 km, the migration of CO₂-rich bubbles that are released from deeper regions of the plumbing system (> 400 MPa) should further promote plagioclase destabilization during their early growth history. Under these circumstances, the spectrum of disequilibrium textures at variable resorption degree that affect the cores of Etnean plagioclases may form in response of different concentrations of CO₂ in the exsolved gas mixture flushing the magmatic system in which crystals grow.

On the same line of evidence, the transfer and injection of prevalent CO₂-rich gas into the shallow reservoirs (< 100 MPa) may have reduced the clinopyroxene stability, causing severe destabilization of their rims. Even in this case, the development of more pervasive disequilibrium features in clinopyroxenes, such as the sieve textures, is consistent with a possible increase of CO₂ concentration in the gas phase flushing the magma stored at shallow crustal levels. Such a process may also explain the occurrence of some sieve textures in plagioclase crystals that cannot be associated to processes of mafic recharge due to the lack of correlation between anorthite, iron and/or magnesium contents (Viccaro et al. 2014).

Acknowledgements

MG acknowledges the PhD fellowship and two PhD research grants from the University of Catania. This work was also supported by a FIR 2014 project from UniCt to MV (grant number 2F119B). F. Vetere wishes to acknowledge the European Research Council (ERC) Consolidator Grant ERC-2013-CoG No. 612776 – CHRONOS and Marie Curie Fellowship IEF SolVoM #297880 to Diego Perugini.

References

- Aiuppa A, Moretti R., Federico C., Giudice G., Gurreri S., Liuzzo M., Papale P., (...), Valenza M. (2007). Forecasting Etna eruption by real time observation of volcanic gas composition. *Geology*, 35:1115-1118
- Aiuppa A, Bertagnini A, Métrich N, Moretti R, Di Muro A, Liuzzo M, Tamburello G (2010a) A model of degassing for Stromboli volcano. *Earth Plan Sci Lett* 295:195-204
- Aiuppa A, Burton M, Caltabiano T, Giudice G, Guerrieri S, Liuzzo M, Mur F, Salerno G (2010b) Unusually large magmatic CO₂ gas emissions prior to a basaltic paroxysm. *Geophys Res Lett* 37:L17303
- Aiuppa A, Lo Coco E, Liuzzo M, Giudice G, Giuffrida G, Moretti R (2016) Terminal Strombolian activity at Etna's central craters during summer 2012: the most CO₂-rich volcanic gas ever recorded at Mount Etna. *Geochem. Journal* 50:123-138
- Allard P (2010) A CO₂-rich gas trigger of explosive paroxysms at Stromboli volcano, Italy. *J Volcanol Geotherm Res* 189:363-374
- Almeev R, Holtz F, Koepke J, Parat F (2012) Experimental calibration of the effect of H₂O on plagioclase crystallization in basaltic melt at 200 MPa. *Amer Mineral* 97:1234-1240
- Almeev R, Holtz F, Ariskin A, Kimura JI (2013) Storage conditions and of Bezymianny volcano parental magmas: Results of phase equilibria experiments 100 and 700 MPa. *Contrib Mineral Petrol* 166:1389-1414

- Aloisi M, Cocina O, Neri G, Orecchio B, Privitera E (2002) Seismic tomography of the crust underneath the Etna Volcano, Sicily. *Phys Earth Plan Int* 134:139-155
- Armienti P, Tonarini S, Innocenti F, D'Orazio M (2007) Mount Etna pyroxene as tracer of petrogenetic processes and dynamics of the feeding system. *Spec Paper Geol Soc Amer* 418:265-276
- Armienti P, Perinelli C, Putirka KD (2013) A new model to estimate deep-level magma ascent rates, with applications to Mt. Etna (Sicily, Italy). *J Petrol* 54:795-813
- Behrens H (1995) Determination of water solubilities in high viscosity silicate glasses. An experimental study on NaAlSi₃O₈ and KAlSi₃O₈ melts. *Eur J Mineral* 7:905-920
- Behrens H, Ohlhorst S, Holtz F, Champenois M (2004) CO₂ solubility in dacitic melts equilibrated with H₂O-CO₂ fluids - Implications for modeling the solubility of CO₂ in silicic melts. *Geochim Cosmochim Acta* 68:4687-4703
- Berndt J, Liebske C, Holtz F, Freise M, Nowak M, Ziegenbein D, Hurkuck W, Koepke J (2002) A combined rapid-quench and H₂-membrane setup for internally heated pressure vessels: Description and application for water solubility in basaltic melts. *Amer Mineral* 87:1717-1726
- Berndt J, Koepke J, Holtz F (2005) Influence of H₂O and oxygen fugacity on differentiation of MORB at 200 MPa. *J Petrol* 46:135-167
- Blundy JD, Cashman KV (2001) Ascent-driven crystallization of dacite magmas at Mount St. Helens, 1980-1986. *Contrib Mineral Petrol* 140:631-650
- Blundy, JD, Cashman KV, Rust A, Witham F (2010) A case for CO₂-rich arc magmas. *Earth Plan Sci Lett* 290:289-301
- Botcharnikov RE, Koepke J, Holtz F, McCammon C, Wilke M (2005) The effect of water activity on the oxidation and structural state of Fe in a ferro-basaltic melt. *Geochim Cosmochim Acta* 69:5071-5085
- Bonaccorso A, Bonforte A, Calvari S, Del Negro C, Di Grazia G, Ganci G, Neri M, Vicari A,

- Boschi E (2011) The initial phases of the 2008-2009 Mount Etna eruption: a multidisciplinary approach for hazard assessment. *J Geophys Res - Solid Earth* 116(3):B03203
- Brey G (1976) CO₂ solubility and solubility mechanisms in silicate melts at high pressures. *Contrib Mineral Petrol* 57:215-221
- Brugger CR, Hummer JE (2010) Crystal size distribution analysis of plagioclase in experimentally decompressed hydrous rhyodacite magmas. *Earth Plan Sci Lett* 300:246-254
- Carmichael ISE, Ghiorso MS (1990). The effect of oxygen fugacity on the redox state of natural liquids and their crystallizing phases. In: Nicholls J, Russel JK (eds), *Reviews in Mineralogy and Geochemistry*, vol. 24. Mineralogical Society of America, Washington, D.C;
- Cashman K (2004) Volatile controls on magma ascent and eruption. In: Sparks R and Hawkesworth C (Eds), *The state of the planet: frontiers and challenges in geophysics*. Amer Geophys Union, 109-124
- Cichy S, Botcharnikov R, Holtz F, Behrens H (2011) Vesiculation and microlite crystallization induced by decompression: A case study of the 1991-1995 Mt. Unzen eruption (Japan). *J Petrol* 52:1469-1492
- Collins SJ, Pyle DM, Maclennan J (2009) Melt inclusions track pre-eruption storage and dehydration of magmas at Etna. *Geology* 37:571-574
- Corsaro RA, Di Renzo V, Di Stefano S, Miraglia L, Civetta L (2013) Relationship between petrologic processes in the plumbing system of Mt. Etna and the dynamics of the eastern flank from 1995 to 2005. *J Volcanol Geotherm Res* 251:75-89
- Dall'Agnol R, Scaillet B, Pichavant M (1999) An experimental study of a lower Proterozoic A-type granite from the Eastern Amazonian craton, Brazil. *J Petrol* 40:1673-1698
- Dingwell DB (1998) Recent experimental progress in the physical description of silicic magma relevant to explosive volcanism. In: Gilbert GS and Sparks RSJ (Eds), *The physics of explosive volcanic eruptions*. Spec Publ Geol Soc London 145:9-26

- Erdmann M, Koepke J (2016) Silica-rich lavas in the oceanic crust: experimental evidence for fractional crystallization under low water activity. *Contrib Mineral Petrol* 171:83
- Feig ST, Koepke J, Snow JE (2006) Effect of water on tholeiitic basalt phase equilibria - an experimental study under oxidizing conditions. *Contrib Mineral Petrol* 152:611-638
- Feig, ST, Koepke J, Snow JE (2010). Effect of oxygen fugacity and water on phase equilibria of a hydrous tholeiitic basalt. *Contrib Mineral Petrol* 160: 551-568;
- Ferlito C, Viccaro M, Cristofolini R (2008) Volatile-induced magma differentiation in the plumbing system of Mt. Etna volcano (Italy): evidence from glass in tephra of the 2001 eruption. *Bull Volcanol* 70:455-473
- Ferlito C, Coltorti M, Lanzafame G, Giacomoni PP (2015) The volatile flushing triggers eruptions at open conduit volcanoes: Evidence from Mount Etna volcano (Italy). *Lithos* 184-187:447-455
- Fiege A, Vetere F, Iezzi G, Simon A, Holtz F (2015) The roles of decompression rate and volatiles ($H_2O+Cl\pm CO_2\pm S$) on crystallization in (trachy-) basaltic magmas. *Chemical Geology* 411:310-322
- Freise M, Holtz F, Nowak M, Scoates JS, Strauss H (2009) Differentiation and crystallization conditions of basalts from the Kerguelen large igneous province: an experimental study. *Contrib Mineral Petrol* 158:505-527
- Ghiorso MS, Gualda GAR (2015) An H_2O-CO_2 mixed fluid solubility model compatible with rhyolite-MELTS. *Contrib Mineral Petrol* 169:53
- Hintzmann W, Müller-Vogt G (1969) Crystal growth and lattice parameters of rare-earth doped yttrium phosphate, arsenate and vanadate prepared by the oscillating temperature flux technique. *J Crystal Growth* 5:274-278
- Housh TB, Lurh JF (1991) Plagioclase-melt equilibria in hydrous system. *Amer Mineral* 76:477-491
- Hummer J, Rutherford M (2002) An experimental study of the kinetics of decompression-induced

crystallization in silicic melts. *J Geophys Res* 107:1-23

Husen A., Almeev R.R., Holtz F. (2016) The Role of H₂O and Pressure on Multiple Saturation and Liquid Lines of Descent in Basalts from the Shatsky Rise, *J Petrology*, doi: 10.1093/petrology/egw008

Iacono-Marziano G, Morizet Y, Le Trong E, Gaillard F (2012) New experimental data and semi-empirical parameterization of H₂O-CO₂ solubility in mafic melt. *Geochim Cosmochim Acta* 97:1-23

Ishibashi H (2013) Spinel-melt oxygen barometry: a method and application to Cenozoic alkali basaltic magmas from the Higashi-Matsuura district, NW Kyushu, Japan. *Geosci Rep Shizuoka Univ* 4:21-32 (in Japanese with English abstract)

Kawamoto T (1992) Dusty and honeycomb plagioclase: indicators of processes in the Uchiho stratified magma chamber, Izu Peninsula, Japan. *J Volcanol Geotherm Res* 49:191-208

Kirkpatrick R (1981) Kinetics of crystallization of igneous rocks. In: Lasaga A and Kirkpatrick R (Eds), *Kinetics of geochemical processes*, *Rev Mineral* 8:321-397, Mineral Soc Amer

Lange RA, Frey HM, Hector J (2009) A thermodynamic model for the plagioclase-liquid hygrometer/thermometer. *Amer Mineral* 94:494-506

Leschik M, Heide G, Frischat GH, Behrens H, Wiedenbeck M, Wagner N, Heide K, Geissler H, Reinholz U (2004) Determination of H₂O and C₂O contents in rhyolitic glasses. *Phys Chem Glasses* 45:238-251

Lofgren GE (1980) Experimental studies on the dynamic of crystallization of silicate melts. Chapter 11. In: Hargraves RB (Ed), *Physics of magmatic processes*, Princeton Univ Press, New Jersey

Martel C, Champallier R, Prouteau G, Pichavant M, Arbaret L, Balcone-Boissard H, Boudon G, Boivin P, Bourdier J, Scaillet B (2013) Trachyte phase relations and implication for magma storage conditions in the Chaîne des Puys (French Massif Central). *J Petrol* 54:1071-1107

Métrich N, Allard P, Spillaert N, Andronico D, Burton MR (2004) 2001 flank eruption of the alkali-

and volatile-rich primitive basalt responsible for Mount Etna's evolution in the last three decades. *Earth Plan Sci Lett* 228:1-17

Mills RD, Ratner JJ, Glazner AF (2011) Experimental evidence for crystal coarsening and fabric development during temperature cycling. *Geology* 39:1139-1142

Mills RD, Glazner AF (2013) Experimental study on the effects of temperature cycling on coarsening of plagioclase and olivine in an alkali basalt. *Contrib Mineral Petrol* 166:97-111

Mollo S, Giacomoni PP, Coltorti M, Ferlito C, Iezzi G, Scarlato P (2015) Reconstruction of magmatic variables governing recent Etnean eruptions: constraints from mineral chemistry and P-T-fO₂-H₂O modelling. *Lithos* 212-215:311-320

Moore GM, Carmichael ISE (1998) The hydrous phase equilibria (to 3 kbar) of an andesite and basaltic andesite from Western Mexico: constraints on water content and conditions of phenocryst growth. *Contrib Mineral Petrol* 130:304-319

Mourtada-Bonnefoi C, Laporte D (2002) Homogeneous bubble nucleation in rhyolitic magma: an experimental study of the effect of H₂O and CO₂. *J Geophys Res* 107(BA)2066

Nelson ST, Montana A (1992) Sieve textured plagioclases in volcanic rocks produced by rapid decompression. *Amer Mineral* 77:1242-1249

Newman S, Lowenstern JB (2002) VolatileCalc: a silicate melt-H₂O-CO₂ solution model written in Visual Basic for Excel. *Comp Geosci* 28:597-604

Nicotra E, Viccaro M (2012a) Transient uprise of gas and gas-rich magma batches fed the pulsating behaviour of the 2006 eruptive episodes at Mt. Etna volcano. *J Volcanol Geotherm Res* 227-228:102-118

Ohuchi T, Nakamura M (2007) Grain growth in the system forsterite-diopside-water. *Phys Earth Plan Int* 161:281-304

Papale P (1997) Thermodynamic modelling of the solubility of H₂O and CO₂ in silicate liquids. *Contrib Mineral Petrol* 126:237-251

Papale P, Dobran F (1994) Magma flow along the volcanic conduit during the Plinian and

- pyroclastic flow phases of the May 18, 1980, Mount St. Helens eruption. *J Geophys Res* 99
- Papale P (1998) Volcanic conduit dynamics. In: Freundt A, Rosi M (Eds), From magma to tephra, modelling physical processes of explosive volcanic eruptions, *Developments in Volcanology Series* 4:55-89, Elsevier New York
- Papale P, Polacci M (1999) Role of carbon dioxide in the dynamics of magma ascent in explosive eruptions. *Bull Volcanol* 60:583-594
- Patanè D, Barberi G, Cocina O, De Gori P, Chiarabba C (2006) Time-resolved seismic tomography detects magma intrusions at Mount Etna. *Science* 313:821-823
- Patanè D, Aiuppa A, Aloisi M, Behncke B, Cannata A, Coltelli M, Di Grazia G, Gambino S, Gurrieri S, Mattia M, Salerno G (2013) Insights into magma and fluid transfer at Mount Etna by a multiparametric approach: A model of the events leading to the 2011 eruptive cycle. *J Geophys Res - Solid Earth* 118:3519-3539
- Pichavant M, Macdonald R (2007) Crystallization of primitive basaltic magmas at crustal pressures and genesis of the calc-alkaline igneous suite: experimental evidence from St Vincent, Lesser Antilles arc. *Contrib Mineral Petrol* 154:535-558
- Pichavant M, Di Carlo I, Rotolo SG, Scaillet B, Burgisser A, Le Gall N, Martel C (2013) Generation of CO₂-rich melts during basalt magma ascent and degassing. *Contrib Mineral Petrol* 166: 545-561.
- Pichavant M, Scaillet B, Pommier A, Iacono-Marziano G, Cioni R (2014) Nature and evolution of primitive Vesuvius magmas: an experimental study. *J Petrol* 55:2281-2310
- Putirka KD (2008) Thermometers and barometers for volcanic systems, In: Putirka K, Tepley J III (Eds), *Rev Mineral Geochem* 69:61-120, Mineral Soc Amer
- Riker JM, Cashman KV, Rust AC, Blundy JD (2015) Experimental constraints on plagioclase crystallization during H₂O- and H₂O-CO₂-saturated magma decompression. *J Petrol* 56(10):1967-1998
- Roeder PL, Emslie RF (1970). Olivine-liquid equilibrium. *Contrib Mineral Petrol* 29:275-289

- Scaillet B, Pichavant M, Roux J, Humbert G, Lefevre A (1992) Improvements of the Shaw membrane technique for measurement and control of fH_2 at high temperatures and pressures. *Amer Mineral* 77:647-655
- Shishkina TA, Botcharnikov RE, Holtz F, Almeev RR, Portnyagin MV (2014a) Solubility of H₂O- and CO₂-bearing fluids in tholeiitic basalts at pressures up to 500 MPa. *Chem Geol* 277:115-125
- Shishkina TA, Botcharnikov RE, Holtz F, Almeev RR, Jazwa AM, Jakubiak AA (2014b) Compositional and pressure effects on the solubility of H₂O and CO₂ in mafic melts. *Chem Geol* 388:112-129
- Spilliaert N, Allard P, Métrich N, Sobolev AV (2006) Melt inclusions record of the conditions of ascent, degassing, and extrusion of volatile-rich alkali basalt during the powerful 2002 flank eruption of Mount Etna (Italy). *J Geophys Res - Solid Earth* 111:B04203.
- Sparks RSJ, Pinkerton H (1978) Effects of degassing on rheology of basaltic lava. *Nature* 276:385-386
- Sparks RSJ (2003) Dynamics of Magma Degassing. In: Oppenheimer C, Pyle DM, Barclay J (Eds), *Volcanic Degassing*, Spec Publ Geol Soc London
- Spera FJ (1981) Carbon dioxide in igneous petrogenesis, II. Fluid dynamics of mantle metasomatism. *Contrib Mineral Petrol* 77:56-65
- Spera FJ (1984) Carbon dioxide in igneous petrogenesis, III. Role of volatiles in the ascent of alkaline magma with special reference to xenolith bearing mafic lavas. *Contrib Mineral Petrol* 88:217-232
- Tanguy JC, Clocchiatti R (1984) The Etnean lavas, 1977-1983: petrology and mineralogy. *Bull Volcanol* 47:879-894
- Tsuchiyama A (1985) Dissolution kinetics of plagioclase in the melt of the system diopside-albite-anorthite, and the origin of dusty plagioclase in andesites. *Contrib Mineral Petrol* 89:1-16
- Tsuchiyama A, Takahashi E (1983) Melting kinetics of a plagioclase feldspar. *Contrib Mineral*

Petrol 84:345-354

- Tuttle OF, Bowen NL (1958) Origin of granite in the light of experimental studies in the system $\text{NaAlSi}_3\text{O}_8\text{-KAlSi}_3\text{O}_8\text{-SiO}_2\text{-H}_2\text{O}$. Geol Soc Amer, Memoir 74, 153 pp
- Vetere F, Botcharnikov RE, Holtz F, Behrens H, De Rosa R (2011) Solubility of H_2O and CO_2 in shoshonitic melts at 1250°C and pressures from 50 to 400 MPa: Implications for Campi Flegrei magmatic systems. J Volcanol Geotherm Res 202:251-261
- Vetere F, Holtz F, Behrens H, Botcharnikov RE, Fanara S (2014) The effect of alkalis and polymerization on the solubility of H_2O and CO_2 in alkali-rich silicate melts. Contrib Mineral Petrol 167:1014
- Vetere F, Mollo S, Giacomoni PP, Iezzi G, Coltorti M, Ferlito C, Holtz F, Perugini D, Scarlato P (2015a) Experimental constraints on the origin of pahoehoe “cicirara” lavas at Mt. Etna volcano (Sicily, Italy). Bull Volcanol 77:44
- Vetere F, Iezzi G, Behrens H, Holtz F, Ventura G, Misiti V, Cavallo A, Mollo S, Dietrich M (2015b) Glass forming ability and crystallization behaviour of sub-alkaline silicate melts. Earth Sci Rev 150:25-44
- Viccaro M, Giacomoni PP, Ferlito C, Cristofolini R (2010) Dynamics of magma supply at Mt. Etna volcano (Southern Italy) as revealed by textural and compositional features of plagioclase phenocrysts. Lithos 116:77-91
- Viccaro M, Garozzo I, Cannata A, Di Grazia G, Gresta S (2014) Gas burst vs. gas-rich magma recharge: a multidisciplinary study to reveal factors controlling triggering of the recent paroxysmal eruptions at Mt. Etna. J Volcanol Geotherm Res 278-279:1-13
- Viccaro M, Calcagno R, Garozzo I, Giuffrida M, Nicotra E (2015) Continuous magma recharge at Mt. Etna during the 2011-2013 period controls the style of volcanic activity and compositions of erupted lavas. Mineral Petrol 109:67-83
- Viccaro M, Barca D, Bohron WA, D’Oriano C, Giuffrida M, Nicotra E, Pitcher BW (2016) Crystal residence time from trace element zoning in plagioclase reveal changes in magma transfer

dynamics at Mt. Etna during the last 400 years. *Lithos* 248:309-323

Giuffrida M, Viccaro M (2017) Three years (2011-2013) of eruptive activity at Mt. Etna: working modes and timescales of the modern volcano plumbing system from micro-analytical studies of crystals. *Earth Sci Rev* 171: 289-322

Webster JD, Kinzler RJ, Mathez EA (1999) Chloride and water solubility in basalt and andesite melts and implications for magmatic degassing. *Geochim Cosmochim Acta* 63:729-738

Webster JD, Vetere F, Botcharnikov R, Goldff B, McBirney A, Doherty AL (2015) Experimental and modeled chlorine solubilities in aluminosilicate melts at 1 to 7000 bars and 700 to 1250 °C. Applications to magmas of Augustine volcano, Alaska. *Amer Mineral* 100(2-3):522-535

Wilson L, Sparks RSJ, Walker GPL (1980) Explosive volcanic eruptions, IV. The control of magma properties and conduit geometry on eruption column behavior. *Geophys J Royal Astronom Soc* 63:117-148

Witham F, Blundy J, Kohn SC, Lesne P, Dixon J, Churakov SV, Botcharnikov R (2011) SolEx: a model for mixed COHSCl-volatile solubilities and exsolved gas compositions in basalt. *Comp Geosci* 45:87-97

Zhang, Y., and Ni, H. (2010) Diffusion of H, C, and O components in silicate melts. *Reviews in Mineralogy and Geochemistry*, 72, 171–225.

Figure Captions

Figure 1 – BSE image of sample S0 that has been used as starting material for experiments of flushing with water and carbon dioxide. S0 has been crystallized from a melt hydrated with 1 wt.% of water. Experiment performed with thermal cycling at $1080^{\circ}\text{C}\pm 20^{\circ}\text{C}$ and pressure of 300 MPa. Cpx = clinopyroxene; plg = plagioclase; ox = opaque oxides.

Figure 2 – Variation of the average Mg# of clinopyroxene and An (mol.%) of plagioclase crystals in the initial sample S0 and for the products flushed at 100 and 300MPa using a fluid with distinct proportion of $\text{H}_2\text{O}+\text{CO}_2$. $X_{\text{CO}_2}^{\text{fl}}$ is the mole fraction of CO_2 in the fluid phase. Bars on data indicate the 2 sigma error.

Figure 3 – Textural characteristic of sample S0 after flushing with a fluid composed of $\text{H}_2\text{O}+\text{CO}_2$ at 300MPa and 1080°C . Experimental results are shown for increasing proportion of CO_2 in the system ($X_{\text{CO}_2}^{\text{fl}}$). Note that in condition of high water activity (lower $X_{\text{CO}_2}^{\text{fl}}$) the mineral assemblage is only constituted by clinopyroxene (cpx) and opaque oxide (ox) in samples 300_S2 and 300_S3. Plagioclase (plg) is found in sample 300_S4, which was flushed with a gas phase at higher CO_2 concentration. Extensive dissolution features can be observed along the plagioclase rims.

Figure 4 – Textural characteristic of sample S0 after flushing with a fluid composed of $\text{H}_2\text{O}+\text{CO}_2$ at 100MPa and 1080°C . Experimental results are shown for increasing mole fraction of CO_2 in the fluid phase, as in Figure 3. Note that as the $X_{\text{CO}_2}^{\text{fl}}$ increases, clinopyroxene crystals show major textural changes and higher degree of resorption, whereas plagioclase crystals do not record significant textural variation.

Figure 5 – Major element compositions of residual glasses for increasing CO₂ composition after flushing experiments at 300MPa and 100MPa. In diagrams the composition of the glass in sample S0 is also shown for comparison.

Table 1. Bulk rock composition of the natural starting material ET12_4M (wt.% anhydrous) determined by Viccaro et al. (2015) and average major oxide composition (wt.%) of the experimental dry glasses and of the starting S0 glass (step 1 experiment) with standard deviations.

	SiO ₂	TiO ₂	Al ₂ O ₃	FeO _{tot}	MnO	MgO	CaO	Na ₂ O	K ₂ O
ET12_4M	47.01	2.02	16.28	12.09	0.22	5.61	11.00	3.33	2.00
Dry glass*	47.37±0.42	1.83±0.03	16.55±0.34	9.86±0.34	0.13±0.03	5.42±0.10	10.60±0.23	3.34±0.69	1.90±0.04
S0 glass**	54.73±0.03	1.55±0.02	19.01±0.13	6.12±0.18	0.23±0.01	3.49±0.06	5.91±0.31	5.26±0.22	3.71±0.03

*average values calculated on 6 electron microprobe analyses

** average values calculated on 5 electron microprobe analyses

Table 2. Experimental conditions, composition of the fluid phase dissolved and exsolved after runs and post run products. Run S₀ at 1080±20°C ; all the other runs at 1080°C.

Run	P (MPa)	log <i>f</i> O ₂	Solid fraction (mg)	Initial fluid fraction XCO ₂ ^{fl} _{in}	Initial fluid compositions (wt. %)		Fluids in the melt (wt. %)*		Exsolved fluids (wt. %)*		Final fluid mole fraction XCO ₂ ^{fl} _{fi}	Post-run products**
					H ₂ O	CO ₂	H ₂ O	CO ₂	H ₂ O	CO ₂		
S ₀	300	-6.95	1000	0	1.1	0	n.a.	n.a.	n.a.	n.a.	0	Cpx+Plg+Ox
300_S2	300	-6.62	20	0.43	3.9	7.3	2.63	0.22	1.27	7.08	0.69	Cpx diss + Ox
300_S3	300	-6.79	15	0.74	3.5	24.9	1.72	0.26	1.78	24.64	0.85	Cpx <i>cryst</i> + Ox
300_S4	300	-7.26	14	0.94	0.7	29.5	0.5	0.28	0.2	29.22	0.98	Cpx cryst + Plg diss +Ox
100_S1	100	-7.01	17	0.24	4.9	3.8	2.39	0.03	2.51	3.77	0.38	Cpx diss Cpx <i>diss</i> + Plg diss + Ox
100_S2	100	-6.82	14	0.51	3.3	8.3	1.58	0.05	1.72	8.25	0.66	Cpx <i>cryst</i> +Plg <i>diss</i> +Ox
100_S4	100	-6.04	15	0.94	0.7	28.8	0.39	0.09	0.31	28.7	0.97	

* Composition calculated through MagmaSat software (Ghiorso and Gualda, 2015).

**In bold: strongly dissolving or crystallizing; in Italics: slight dissolving or crystallizing

Fig. 1

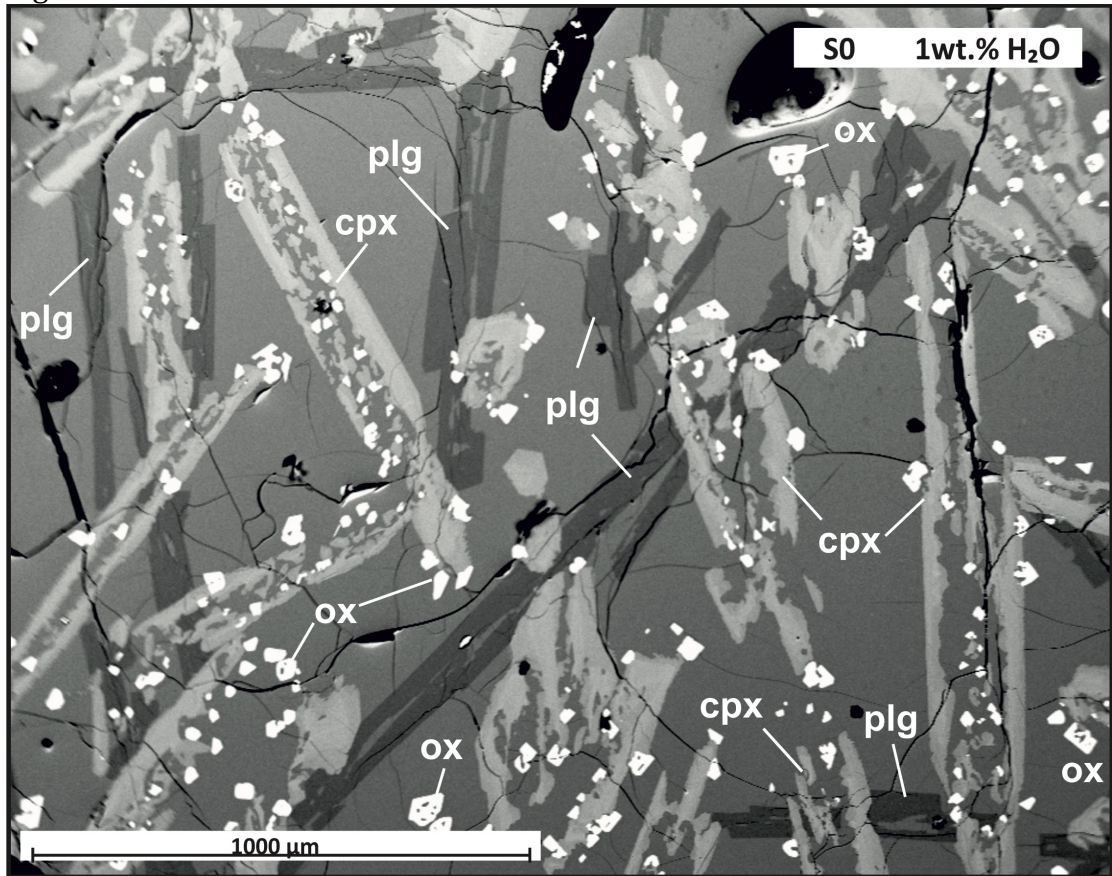


Fig. 2

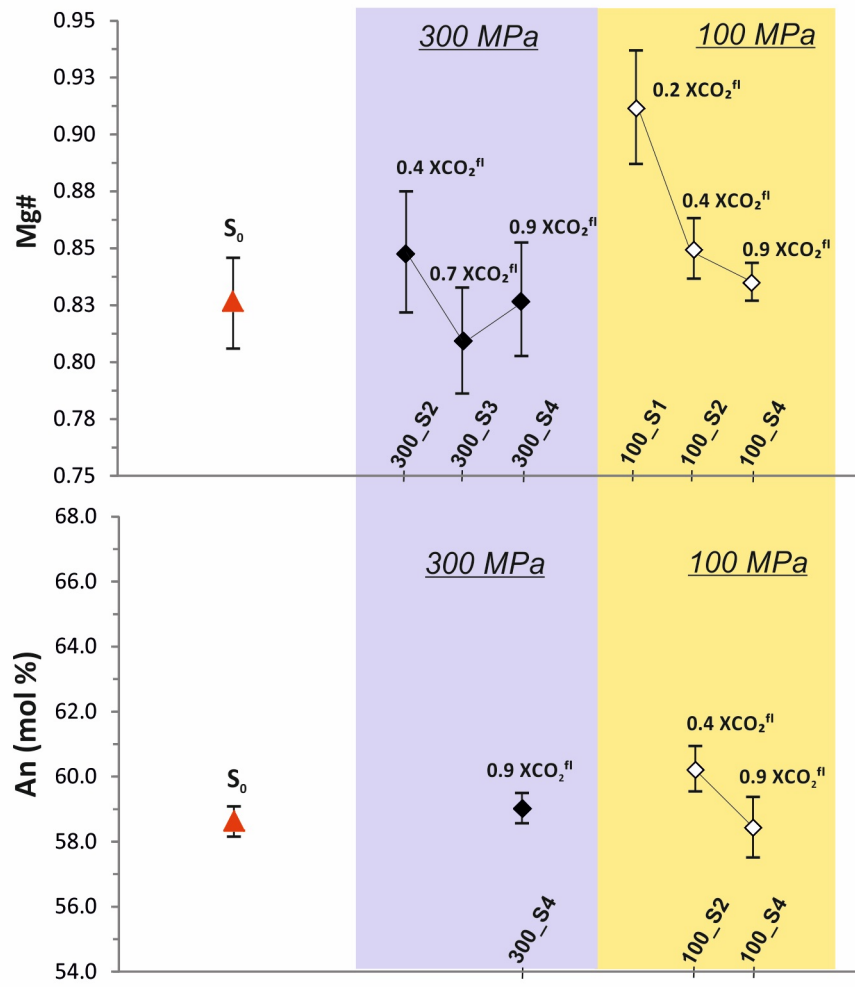


Fig. 3

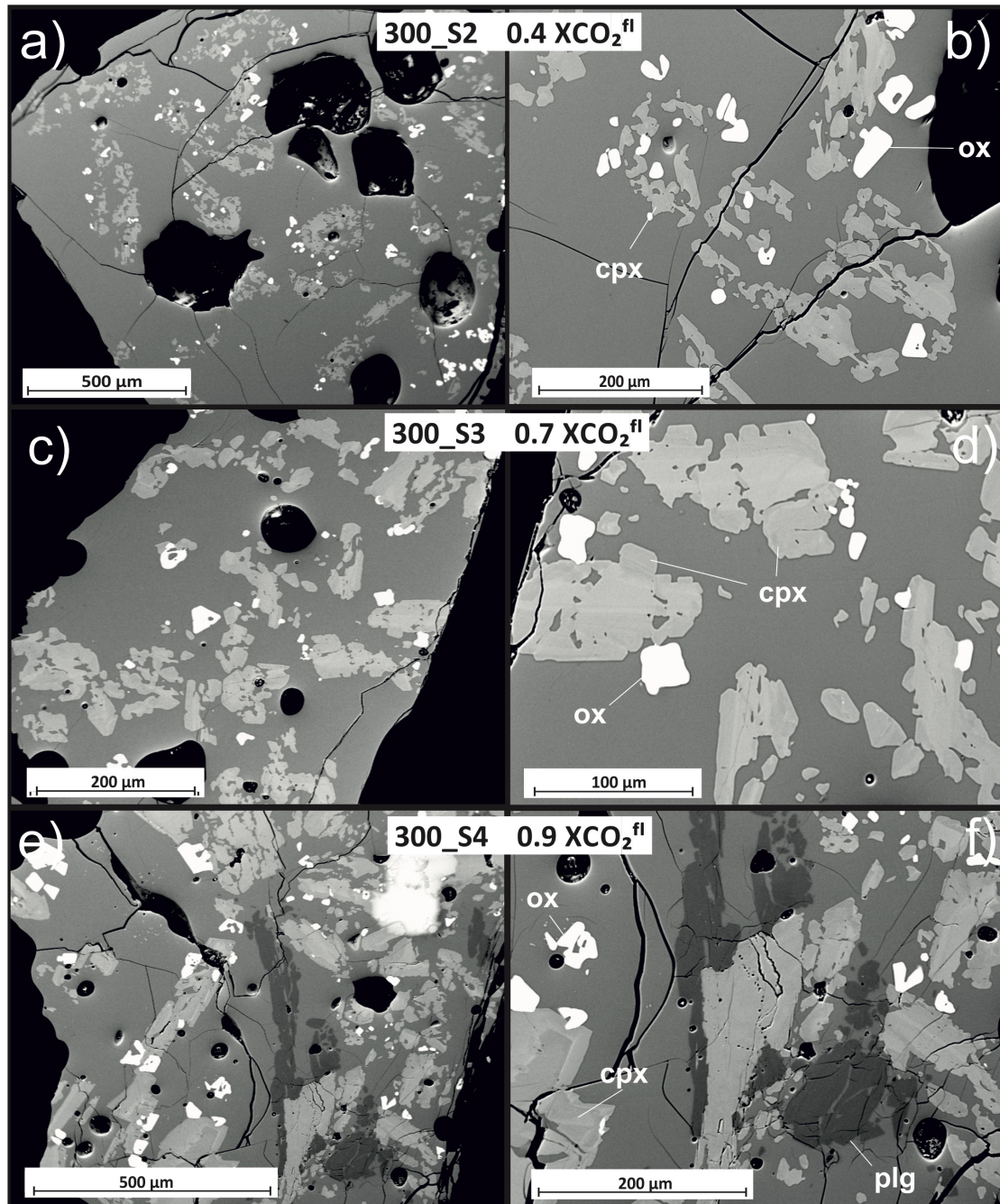


Fig. 4

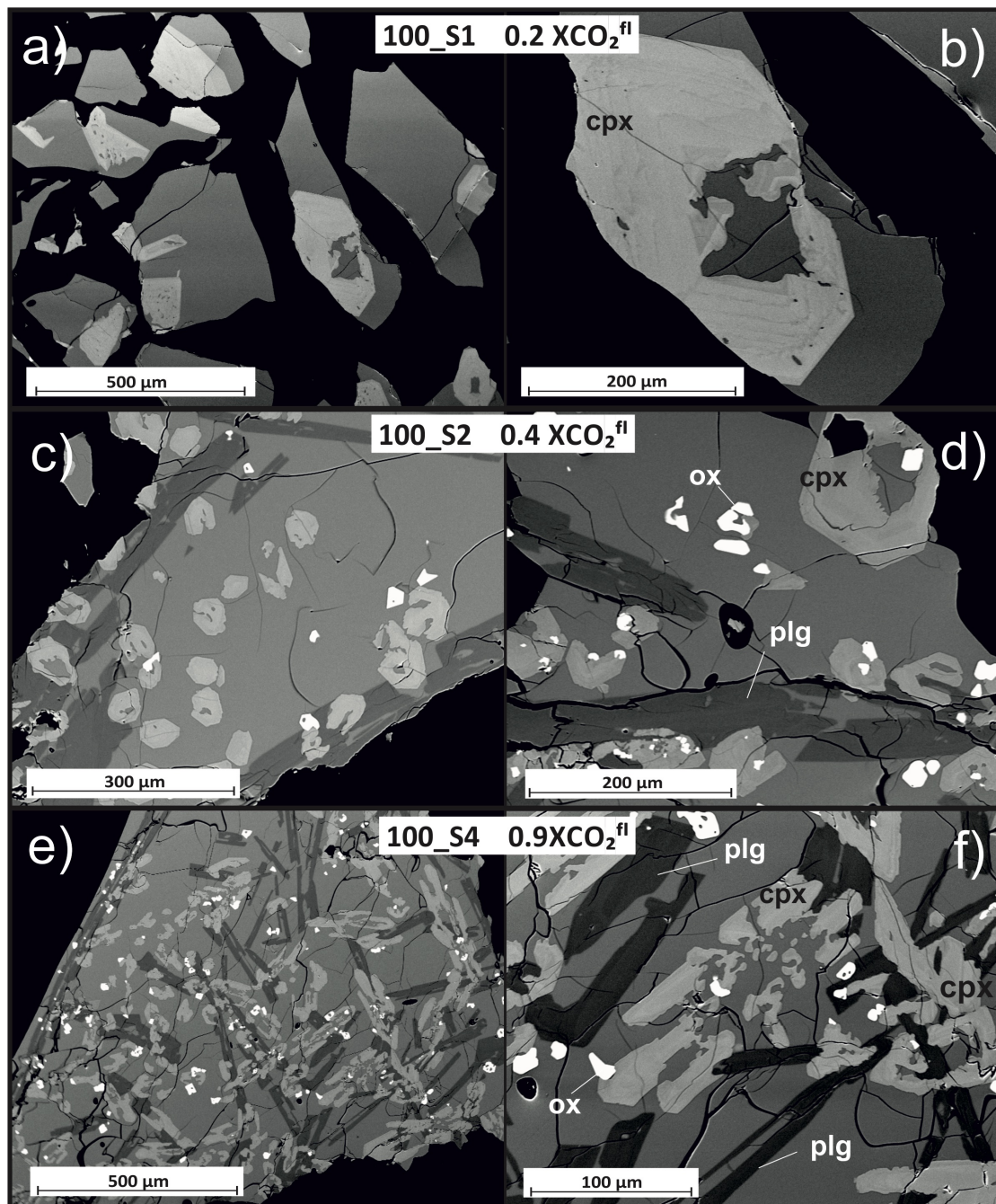


Fig. 5

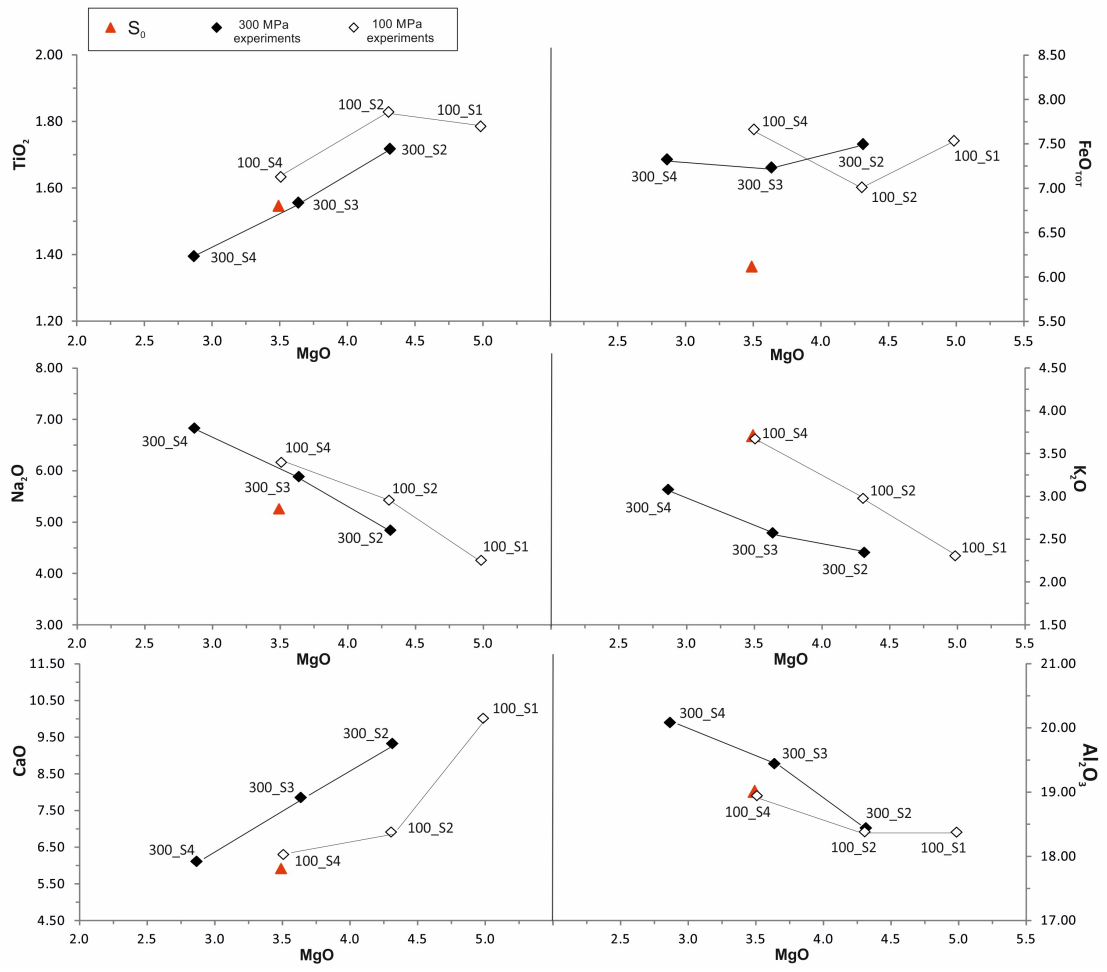


Fig. 6

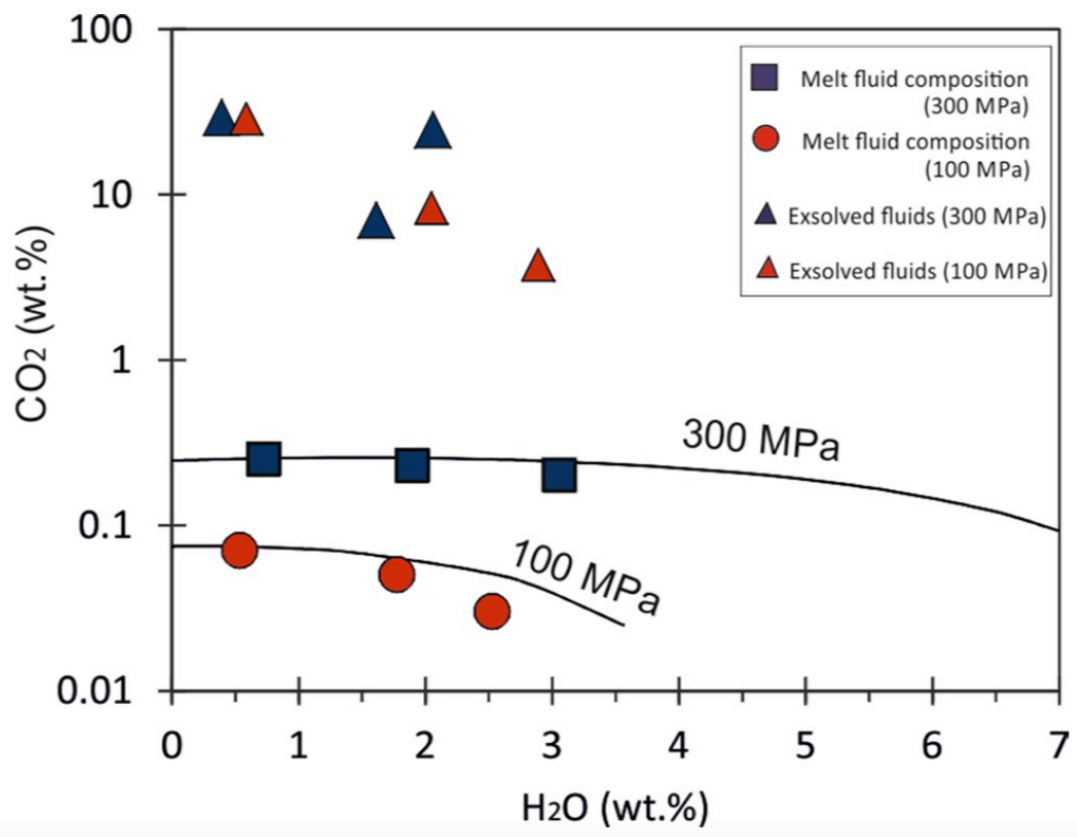
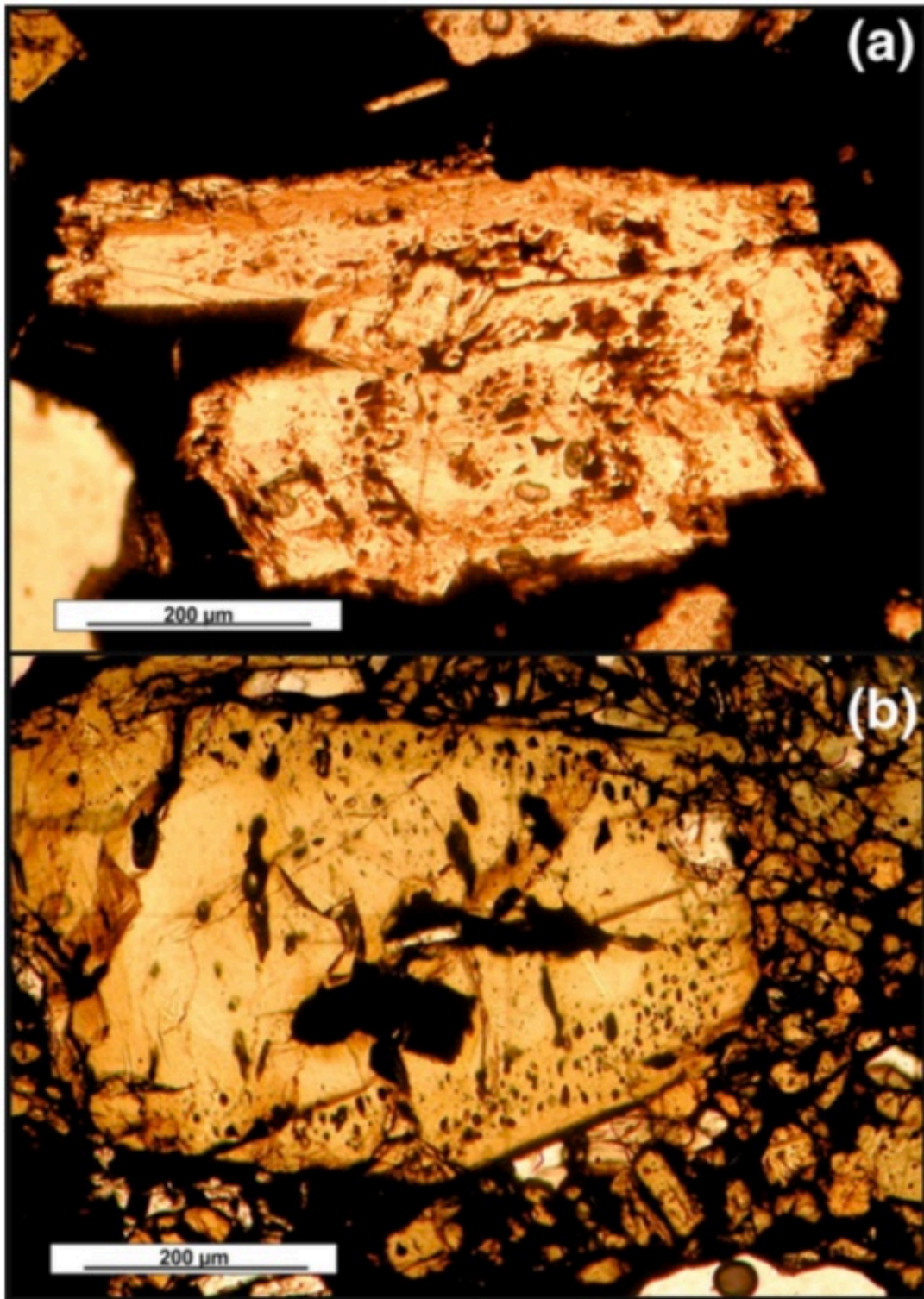


Fig. 7



Major oxide composition of the experimental glasses

H2O-bearing system

50

Experimental conditions: 1 wt.% H2O; Thermal Cycling 76h 1080±20 °C; P=300 MPa.

spots	SiO ₂	TiO ₂	Al ₂ O ₃	FeO	MnO	MgO	CaO	Na ₂ O	K ₂ O	Total
A1	54.71	1.56	19.19	5.96	0.24	3.53	5.67	5.36	3.78	100.00
A2	54.61	1.46	18.93	6.14	0.24	3.62	6.32	5.04	3.64	100.00
A3	54.74	1.63	19.18	5.88	0.20	3.57	5.96	5.03	3.80	100.00
A4	54.84	1.52	18.98	6.19	0.29	3.31	5.98	5.26	3.63	100.00
A5	54.75	1.56	18.77	6.42	0.16	3.44	5.63	5.59	3.69	100.00
Average	54.73	1.55	19.01	6.12	0.23	3.49	5.91	5.26	3.71	100.00

H2O+CO2-bearing system

300_52Experimental conditions: 0.4 XCO₂^{fl}; P=300 Mpa; T 1100°C

spots	SiO ₂	TiO ₂	Al ₂ O ₃	FeO	MnO	MgO	CaO	Na ₂ O	K ₂ O	Total
A2	51.42	1.73	18.49	7.29	0.02	4.31	9.59	4.84	2.32	100.00
A3	51.33	1.86	18.71	7.49	0.14	4.33	9.29	4.33	2.52	100.00
A4	51.55	1.64	18.67	7.66	0.12	4.27	9.04	4.79	2.25	100.00
A5	51.97	1.64	17.95	7.59	0.04	4.08	9.38	4.91	2.43	100.00
A6	50.80	1.72	18.36	7.45	0.24	4.58	9.33	5.33	2.19	100.00
average	51.42	1.72	18.44	7.49	0.11	4.31	9.32	4.84	2.35	100.00

300_53Experimental conditions: 0.7 XCO₂^{fl}; P=300 Mpa; T 1100°C

spots	SiO ₂	TiO ₂	Al ₂ O ₃	FeO	MnO	MgO	CaO	Na ₂ O	K ₂ O	Total
A1	51.98	1.59	19.44	7.00	0.06	3.61	7.75	5.93	2.65	100.00
A2	51.24	1.52	19.45	7.14	0.22	3.56	7.98	6.36	2.54	100.00
A3	50.96	1.60	19.44	7.56	0.20	3.60	8.27	5.87	2.51	100.00
A4	52.11	1.50	19.14	7.42	0.12	3.76	7.59	5.67	2.69	100.00
A5	52.04	1.57	19.73	7.04	0.22	3.66	7.67	5.59	2.47	100.00
average	51.67	1.56	19.44	7.23	0.16	3.64	7.85	5.88	2.57	100.00

300_54Experimental conditions: 0.9 XCO₂^{fl}; P=300 Mpa; T 1100°C

spots	SiO ₂	TiO ₂	Al ₂ O ₃	FeO	MnO	MgO	CaO	Na ₂ O	K ₂ O	Total
A1	52.36	1.39	19.92	7.15	0.04	2.90	5.81	7.37	3.06	100.00
A2	51.76	1.38	20.04	7.60	0.12	2.85	6.35	6.84	3.06	100.00
A3	52.65	1.39	19.84	7.21	0.12	2.79	6.16	6.62	3.23	100.00
A4	51.77	1.42	20.31	7.08	0.35	2.91	6.29	6.90	2.96	100.00
A5	52.20	1.40	20.30	7.58	0.22	2.87	5.94	6.41	3.08	100.00
average	52.15	1.39	20.08	7.32	0.17	2.87	6.11	6.83	3.08	100.00

100_51Experimental conditions: 0.2 XCO₂^{fl}; P=100 Mpa; T 1100°C

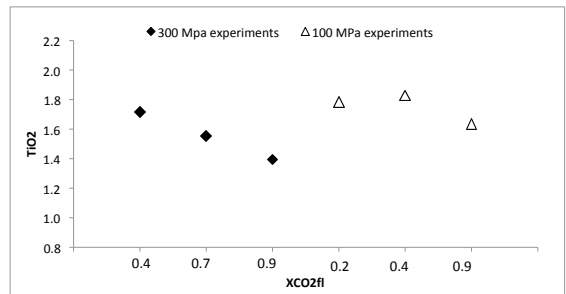
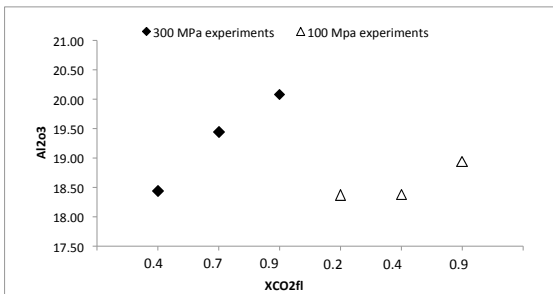
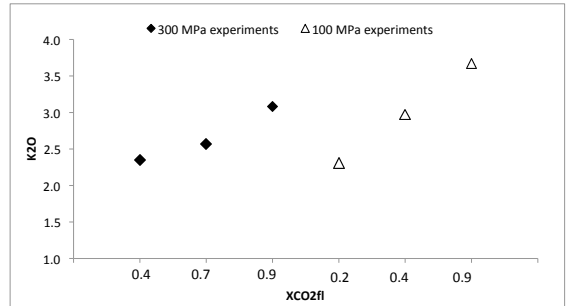
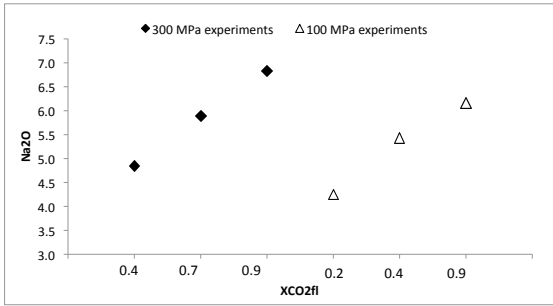
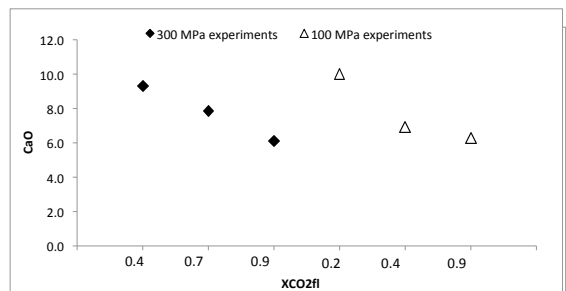
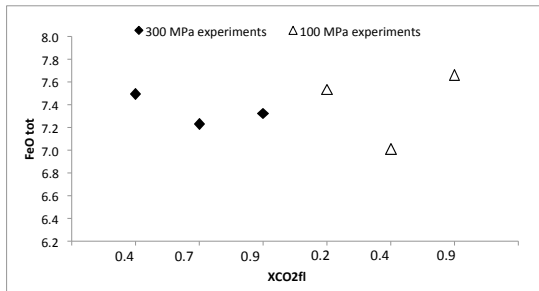
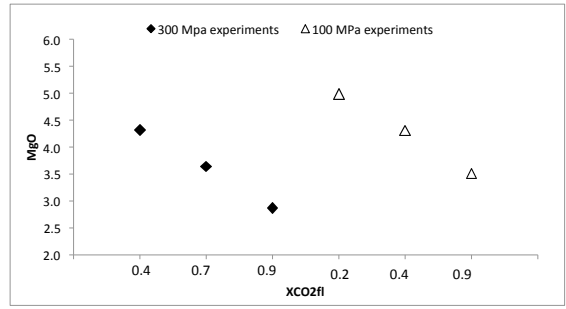
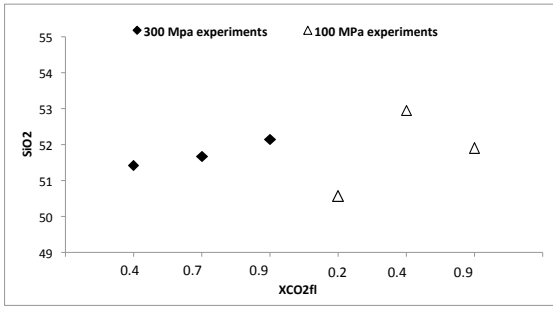
spots	SiO ₂	TiO ₂	Al ₂ O ₃	FeO	MnO	MgO	CaO	Na ₂ O	K ₂ O	Total
A1	50.29	1.83	18.50	7.43	0.26	5.16	9.95	4.25	2.34	100.00
A2	50.74	1.79	18.25	7.73	0.11	4.96	10.17	3.99	2.26	100.00
A3	50.47	1.77	18.40	7.75	0.29	4.87	9.81	4.37	2.26	100.00
A4	50.50	1.78	18.24	7.71	0.16	4.88	10.01	4.43	2.30	100.00
A5	50.82	1.76	18.47	7.05	0.15	5.06	10.11	4.23	2.35	100.00
average	50.57	1.78	18.37	7.53	0.19	4.99	10.01	4.25	2.30	100.00

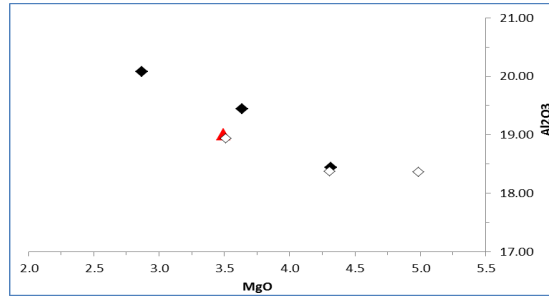
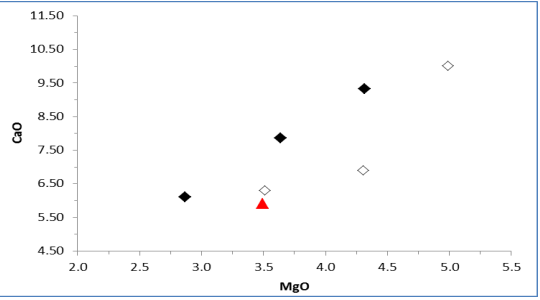
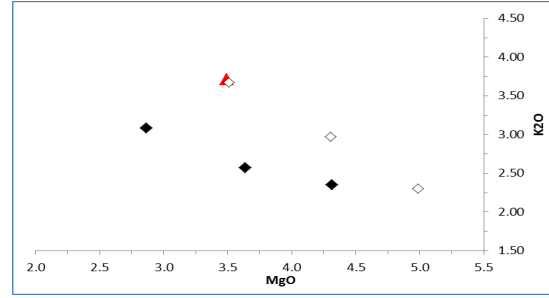
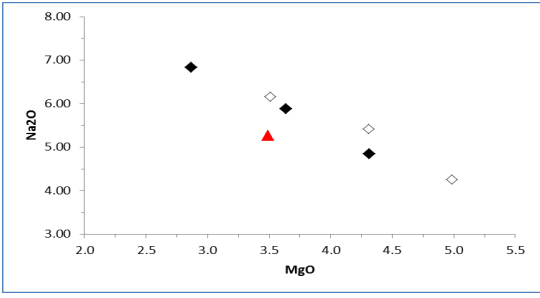
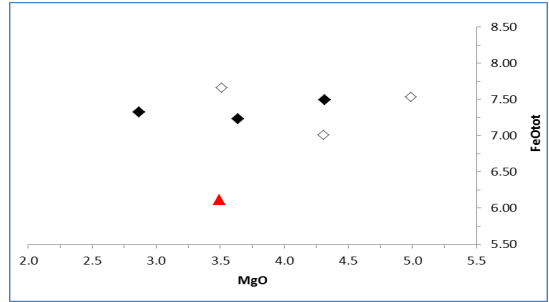
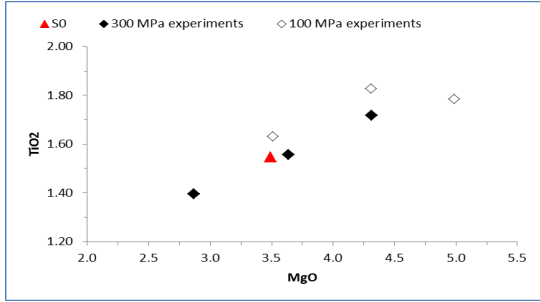
100_52Experimental conditions: 0.4 XCO₂^{fl}; P=100 Mpa; T 1100°C

spots	SiO ₂	TiO ₂	Al ₂ O ₃	FeO	MnO	MgO	CaO	Na ₂ O	K ₂ O	Total
A1	53.20	1.78	18.43	6.96	0.25	4.12	6.96	5.36	2.95	100.00
A2	52.81	1.81	18.63	6.91	0.26	4.24	6.90	5.56	2.88	100.00
A3	52.86	1.93	18.22	7.04	0.26	4.42	6.73	5.52	3.03	100.00
A4	52.91	1.80	18.23	7.13	0.14	4.45	7.05	5.25	3.04	100.00
average	52.95	1.83	18.38	7.01	0.23	4.31	6.91	5.42	2.97	100.00

100_54Experimental conditions: 0.9 XCO₂^{fl}; P=100 Mpa; T 1100°C

spots	SiO ₂	TiO ₂	Al ₂ O ₃	FeO	MnO	MgO	CaO	Na ₂ O	K ₂ O	Total
A1	52.32	1.71	18.71	7.69	0.14	3.53	6.40	5.88	3.62	100.00
A2	51.47	1.71	19.09	7.80	0.17	3.60	6.38	6.13	3.65	100.00
A3	51.95	1.56	19.08	7.66	0.26	3.54	6.18	6.13	3.64	100.00
A4	51.83	1.66	18.85	7.69	0.28	3.42	6.43	6.10	3.74	100.00
A5	51.87	1.57	18.99	7.39	0.17	3.58	6.30	6.45	3.70	100.00
A6	51.99	1.58	18.92	7.75	0.32	3.39	6.10	6.28	3.67	100.00
average	51.90	1.63	18.94	7.66	0.22	3.51	6.30	6.16	3.67	100.00





Mineral assemblage and composition of the experimental samples

Programme: Fplagjagde; Overage: ends

H2O-bearing system

Experimental conditions: 1 wt.% H₂O, Thermal Cycling 700 - 1000/30 °C, P=300 MPa

Table with columns: Sample, SiO2, TiO2, Al2O3, FeO, MnO, MgO, CaO, Na2O, K2O, Total, Diopside, Anorthite, Jadeite, Opa, Tschermakite, Mg#

Table with columns: Sample, SiO2, TiO2, Al2O3, FeO, MnO, MgO, CaO, Na2O, K2O, Total, An% (Ank, AnC), Opa%

Table with columns: Sample, SiO2, TiO2, Al2O3, FeO, MnO, MgO, CaO, Na2O, K2O, Total, An% (Ank, AnC), Opa%

H2O-CO2-bearing system

Experimental conditions: 0.4 K2O, P=300 MPa, T=1100°C

Table with columns: Sample, SiO2, TiO2, Al2O3, FeO, MnO, MgO, CaO, Na2O, K2O, Total, Diopside, Anorthite, Jadeite, Opa, Tschermakite, Mg#

Table with columns: Sample, SiO2, TiO2, Al2O3, FeO, MnO, MgO, CaO, Na2O, K2O, Total, An% (Ank, AnC), Opa%

Table with columns: Sample, SiO2, TiO2, Al2O3, FeO, MnO, MgO, CaO, Na2O, K2O, Total, An% (Ank, AnC), Opa%

Table with columns: Sample, SiO2, TiO2, Al2O3, FeO, MnO, MgO, CaO, Na2O, K2O, Total, An% (Ank, AnC), Opa%

Table with columns: Sample, SiO2, TiO2, Al2O3, FeO, MnO, MgO, CaO, Na2O, K2O, Total, An% (Ank, AnC), Opa%

Table with columns: Sample, SiO2, TiO2, Al2O3, FeO, MnO, MgO, CaO, Na2O, K2O, Total, An% (Ank, AnC), Opa%

Table with columns: Sample, SiO2, TiO2, Al2O3, FeO, MnO, MgO, CaO, Na2O, K2O, Total, An% (Ank, AnC), Opa%

Table with columns: Sample, SiO2, TiO2, Al2O3, FeO, MnO, MgO, CaO, Na2O, K2O, Total, An% (Ank, AnC), Opa%

Table with columns: Sample, SiO2, TiO2, Al2O3, FeO, MnO, MgO, CaO, Na2O, K2O, Total, An% (Ank, AnC), Opa%

Table with columns: Sample, SiO2, TiO2, Al2O3, FeO, MnO, MgO, CaO, Na2O, K2O, Total, An% (Ank, AnC), Opa%

Table with columns: Sample, SiO2, TiO2, Al2O3, FeO, MnO, MgO, CaO, Na2O, K2O, Total, An% (Ank, AnC), Opa%

Table with columns: Sample, SiO2, TiO2, Al2O3, FeO, MnO, MgO, CaO, Na2O, K2O, Total, An% (Ank, AnC), Opa%

Table with columns: Sample, SiO2, TiO2, Al2O3, FeO, MnO, MgO, CaO, Na2O, K2O, Total, An% (Ank, AnC), Opa%